Advanced Model for Turbulent Gas–Solid Flow and Reaction in FCC Riser Reactors

Jinsen Gao, Chunming Xu, Shixiong Lin, and Guanghua Yang
State Key Laboratory of Heavy Oil Processing, University of Petroleum, Beijing, 102200, P.R. China

Yincheng Guo
Dept. of Engineering Mechanics, Tsinghua University, Beijing, 100084, P.R. China

A 3-D two-phase flow-reaction model was developed for predicting the performance of FCC riser reactors. This model combines two-phase turbulent flow with 13-lump reaction kinetics. The simulated results show that the gas– particulate turbulent reacting flow regime in the riser reactor is extremely complex, especially at the feed inlet zone of the riser reactor. The distributions of velocities, temperature, and yields are not homogeneous in the riser reactor. The model predictions were used as a design tool for operational case studies. The optimum yields of desirable FCC products, gasoline and light fuel oil were achieved at a critical riser height that is less than 10 m above the feed inlet. Beyond the critical riser height, excessive cracking reactions resulted in the increased yields of by-products, cracking gas and coke, at the expense of desirable products. Model simulations carried out to determine the parametric effects on product yields suggest that injection of water as a reaction-terminating medium above the critical riser height can be an effective option for optimizing the yields of desirable products.

Introduction

Fluid catalytic cracking (FCC) is the workhorse of modern refinery worldwide. Its function is to convert heavy petroleum fractions into more usable products such as gasoline, middle distillates, and light olefins. An FCC unit consists of two key units: a reactor and a regenerator. In the reactor, the hot regenerated catalyst is brought in contact with feed oil where catalytic cracking reactions take place. In the regenerator, the spent catalyst is regenerated by burning off the coke formed in the reactor. Both the catalytic cracking reactions and catalyst regeneration are carried out in fluidized beds. The heat of coke combustion in the regenerator also heats up the catalyst, which provides the heat required for heating and evaporating the feed, as well as for endothermic heat of the cracking reactions (Arbel et al., 1995).

The FCC is still an evolving technology since the first commercialization over a half of century ago. Improvements in the technology as well as changing feedstocks and product requirements continue to drive this evolution. A successful effort is the development of new, very active zeolite cracking catalysts that allowed the cracking reactions to be completed in short-contact-time riser reactors. The catalyst is pneumatically conveyed by steam and hydrocarbon vapors from the bottom to the top. During this conveying process, efficient mixing and contact of catalyst with hydrocarbons enhance the catalytic cracking reactions. The riser reactor becomes the key part of an FCC unit since its operation can dominate the product distribution and quality (Chen and Cao, 1995). Considerable effect has been devoted to better understanding the complexity of riser reactor, including theoretical and experimental study, pilot plant, and commercial tests.

Typical superficial gas and solids velocity in the commercial riser reactor is 7–15 m/s. This results in gas–particle two-phase turbulence flow. In addition, many complicated processes such as catalytic cracking, heat transfer, and mass transfer are involved in the commercial risers. This is commonly referred to as turbulent gas–particle flow with reaction (Guo, 1995). Another special aspect of the riser reactor is the feed nozzles, which are uniformly spaced around the

Correspondence concerning this article should be addressed to J. Gao.

circumference. The feed oil and atomizing steam are injected obliquely upwards into the riser reactor, forming high-velocity efflux. The riser reactor is divided into two zones with different functions. One is the feed-injecting zone at the bottom of the riser, where the catalyst is accelerated and the evaporation of feed oil takes place and catalytic cracking reaction is initiated. The other is the middle and upper sections (Gates et al., 1979; Mauleon and Courelle, 1985).

The feed-injecting zone is the most complex part of the riser reactor, where intense turbulence and flow inhomogeneities originated from the efflux with high velocity of feed oil and atomizing steam, resulting in high velocity, temperature, and concentration gradients. Some researchers (Merry, 1971; Chen and Weinstein, 1993) showed that the directed feed jets introduced into a fluidized-bed reactor have a considerable effect on the hydrodynamic behavior of the reactor. The jet can form a coherent void, bubble trains, and a surrounding compaction zone.

Moreover the hot spots at the inlet zone promote the secondary cracking reactions that produce undesirable light hydrocarbons and coke. Many efforts have been made in feed-injection design to control the flow of catalyst and hydrocarbons at plug-flow conditions in order to minimize the undesirable temperature gradients, which may result in undesirable cracking reaction (McKetta, 1981; Yen et al., 1985; Mauleon and Courelle, 1985). In addition, the complex geometry and hydrodynamics, as mentioned earlier, break the circumference uniformity of the gas-particle flow in the riser. Hence, a full-scale 3-D model is required to describe the commercial riser reactor.

Until recently, most of the work on the FCC riser reactor was focused on either reactor hydrodynamics or catalytic cracking kinetics. Many theoretical and experimental studies are carried out to better understand the complex hydrodynamics of two-phase turbulent flow in vertical or nonvertical transfer lines (Bader et al., 1988; Chen and Wood, 1985; Hartage et al., 1988; Ocone et al., 1993; Sinclair and Jackson, 1989; Dasgupta et al., 1994; Gidaspow and Ettehadieh, 1983; Ma and Ahmad, 1990; Nieuwland et al., 1996; Samuelsberg and Hjertager, 1996; Pita and Sundareson, 1993; Miller and Gidaspow, 1992; Wang et al., 1993), which are used not only in riser catalytic cracking, but also in other industrial applications. Most of the experiments were carried out in cold flow modes, excluding the influence of heat transfer and cracking reactions. But Saxtoll and Worley (1970) reported nonuniform distribution of catalyst concentration across the riser cross sections in a pilot-plant unit. Schuurmans (1980) measured the radial distribution of catalyst concentration in a modern catalytic cracking rise reactor using the gamma-ray technique. He also obtained a typical conversion profile along the riser height.

Numerous articles on catalytic cracking kinetics can be found in the published literature, with various forms of reaction schemes of varying complexity. On the basis of the lumping theory developed by Wei and Prater (1962, 1963), Weekman (1970) established a fundamental three-lump kinetic model for the vacuum gas oil feed. Paraskos et al. (1976) and Yen et al. (1988) proposed three-lump kinetics, and Lee et al. (1989) proposed a four-lump kinetic model. They are similar to Weekman (1970). Takatsuka et al. (1987) fitted the experimental data with a six-lump kinetics for feed blended with vacuum residua. Jacob et al. (1976) developed a more detailed ten-lump kinetic model to take into account other feed properties in addition to boiling range. Other reaction kinetic schemes of greater complexity have been considered by Sa et al. (1985), Zhu et al. (1985), Mao et al. (1985), and Sa et al. (1995), proposing eleven-lump kinetic models for vacuum gas oil feed and thirteen-lump kinetic models for residua feed.

For all kinetic models just reviewed, isothermal plug-flow is commonly assumed for the flow pattern of the riser reactor to integrate the model equation for predicting of yields, except by Takatsuka et al. (1987), who only adopted a 5-stage CSTR model to adjust the backmixing. In other words, a mathematical model of an FCC riser reactor from a kinetic scheme focuses only on the cracking reaction, without considering the complicated turbulent flow and heat-transfer configuration. Such a mathematical model deduced from the mechanical cracking kinetic is apt to be rather empirical (Jacob et al., 1976; Mao et al., 1985).

Momentum transfer, heat transfer, and catalytic cracking reactions in commercial units are known to be interrelated, especially in the inlet zone (Chen and Cao, 1995). It appears that an overall study on the gas–particle turbulent flow, heat transfer, and cracking reaction in the riser reactor should be an important engineering aspect of catalytic cracking in the riser reactors (Chen, 1985).

Until now, not much effort has been devoted to this aspect. In recent studies by Theologos and Markatos (1993) and Theologos et al. (1997), a computational fluid-dynamic model was proposed that included the simultaneous interaction of gas–particle flow and catalytic cracking. They did not consider turbulent flow and the diffusion of particle phase, but assuming that the turbulent viscosity of the gas phase is 1,000 times the laminar viscosity and using three-lump kinetics or ten-lump kinetics only suitable for the riser reactors with vacuum gas oil feedstocks.

In the present study, a three-dimensional two-phase turbulent flow-reaction model was developed based on a modified two-phase turbulent model for the comparatively dense particle phase and incorporating thirteen-lump kinetics of the residuum cracking reaction (Sa et al., 1995). Predicted results are compared with the operating data for the commercial riser reactor. The turbulent flow-reaction model is also used to assess the effect of operation optimum, design modification, and so forth.

Physical and Mathematical Model

The realistic picture of the mechanical behavior of such a system must include a variety of interactions that depend on the two-phase flow and reaction. After the feed is injected into the riser reactor, feed oil immediately evaporates due to intimate contact with the regenerated catalyst at a high temperature and intensive interphase heat transfer. The feed spray is formed in the inlet zone, where the high-velocity efflux promotes the turbulence of gas–particle two-phase flow reaction, which greatly influences the resulting heat transfer and catalytic cracking reactions. Hence the physical model of the gas–particulate turbulent flow-reaction in FCC riser reactors should include all components shown in Figure 1. This physical model depicts the coupling and correlation of the

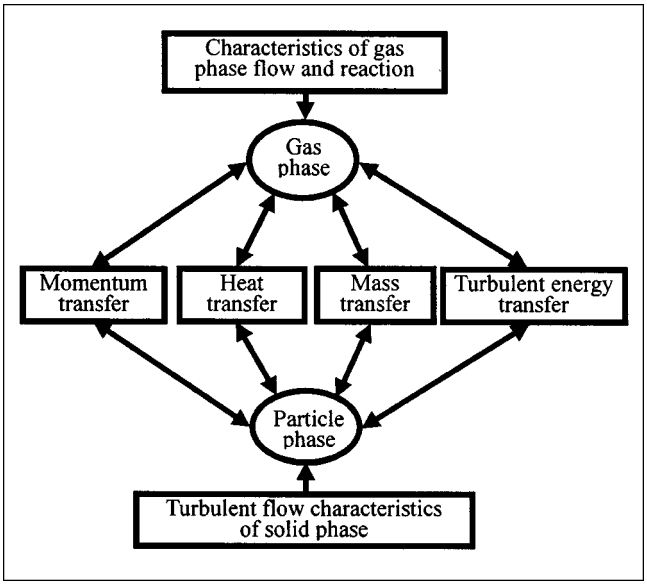

Figure 1. Physical model of FCC riser reactors.

turbulent flow, heat transfer, and catalytic cracking reaction between the gas and particle phases.

Governing equations

The gas–particle two-phase turbulent flow-reaction model is developed based on the Eulerian two-fluid approach (Zhou and Huang, 1990; Gao, 1995), in which both the gas and particulate phases are considered as a continuum. Instantaneous vaporization of the feed is assumed when it enters the riser reactor. The regenerated catalysts provide the heat of vaporization. The instantaneous governing equations of the two-phase flow-reaction model for mass, momentum, heat, and species in an FCC riser reactor can be written in the following forms:

For the gas phase:

$$\frac{\partial}{\partial t}(\epsilon_g \rho_g) + \frac{\partial}{\partial x_j}(\epsilon_g \rho_g v_j) = 0 \tag{1}$$

$$\frac{\partial}{\partial t}(\epsilon_g \rho_g v_i) + \frac{\partial}{\partial x_j}(\epsilon_g \rho_g v_i v_j) = -\epsilon_g \frac{\partial p}{\partial x_i} + \frac{\partial}{\partial x_j} \times \left[\mu\left(\frac{\partial v_i}{\partial x_j} + \frac{\partial v_j}{\partial x_i}\right)\right] + \epsilon_g \rho_g g_i + \frac{\rho_P}{\tau_{rP}}(v_{Pi} - v_i) \tag{2}$$

$$\frac{\partial}{\partial t}(\epsilon_g \rho_g C_P T) + \frac{\partial}{\partial x_j}(\epsilon_g \rho_g v_j C_P T) = \frac{\partial}{\partial x_j}\left(\lambda \frac{\partial T}{\partial x_j}\right) - W_s Q_R + n_P Q_P \tag{3}$$

$$\frac{\partial}{\partial t}(\epsilon_g \rho_g Y_s) + \frac{\partial}{\partial x_j}(\epsilon_g \rho_g v_j Y_s) = \frac{\partial}{\partial x_j}\left(\epsilon_g \rho_g D \frac{\partial Y_s}{\partial x_j}\right) + W_s. \tag{4}$$

For the particulate phase:

$$\frac{\partial}{\partial t}(\rho_P) + \frac{\partial}{\partial x_j}(\rho_P v_{Pj}) = 0 \tag{5}$$

$$\frac{\partial}{\partial t}(\rho_P v_{Pi}) + \frac{\partial}{\partial x_j}(\rho_P v_{Pj} v_{Pi}) = -\epsilon_P \frac{\partial p}{\partial x_i} + \rho_P g_i + \frac{\rho_P}{\tau_{rP}}(v_i - v_{Pi}) \tag{6}$$

$$\frac{\partial}{\partial t}(\rho_P C_{PP} T_P) + \frac{\partial}{\partial x_j}(\rho_P v_{Pj} C_{PP} T_P) = -n_P Q_P. \tag{7}$$

In practice, because the FCC riser reactor is under turbulent flow conditions, it is necessary to use proper turbulent models to describe the effects of the turbulent fluctuation of velocity and scalar variables for the basic conservation equations.

The conservation equations for turbulent flows can be obtained from the basic governing equations using Reynolds averaging. The Reynolds-averaging procedure divided a conserved scalar value ϕ into a mean value $\overline{\phi}$ and a fluctuation part ϕ':

$$\phi = \overline{\phi} + \phi'. \tag{8}$$

Substituting Eq. 8 into the general conservation, Eqs. 1 to 7, and taking the time average over a long period of time yields the moment, heat, and species balance equations. A set of Reynolds-averaged conservation equations for the mass, heat, momentum, and chemical species for the two-phase reaction could be written as follows.

For the gas phase:

$$\frac{\partial}{\partial t}(\epsilon_g \rho_g) + \frac{\partial}{\partial x_j}(\epsilon_g \rho_g v_j) = 0 \tag{9}$$

$$\frac{\partial}{\partial t}(\epsilon_g \rho_g v_i) + \frac{\partial}{\partial x_j}(\epsilon_g \rho_g v_i v_j) = -\epsilon_g \frac{\partial P}{\partial x_i} + \frac{\partial}{\partial x_j}\left[\mu\left(\frac{\partial v_i}{\partial x_j} + \frac{\partial v_j}{\partial x_i}\right)\right] + \epsilon_g \rho_g g_i + \frac{\rho_P}{\tau_{rP}}(v_{Pi} - v_i) - \frac{\partial}{\partial x_j}\left(\epsilon_g \rho_g \overline{v_i' v_j'}\right) \tag{10}$$

$$\frac{\partial}{\partial t}(\epsilon_g \rho_g C_P T) + \frac{\partial}{\partial x_j}(\epsilon_g \rho_g v_j C_P T) = \frac{\partial}{\partial x_j}\left(\lambda \frac{\partial T}{\partial x_j}\right) - W_s Q_R + n_P Q_P - \frac{\partial}{\partial x_j}\left(\epsilon_g \rho_g C_P \overline{v_j' T'}\right) \tag{11}$$

$$\frac{\partial}{\partial t}(\epsilon_g \rho_g Y_s) + \frac{\partial}{\partial x_j}(\epsilon_g \rho_g v_j Y_s) = \frac{\partial}{\partial x_j}\left(\epsilon_g \rho_g D \frac{\partial Y_s}{\partial x_j}\right) + W_s - \frac{\partial}{\partial x_j}\left(\epsilon_g \rho_g \overline{v_j' Y_s'}\right). \tag{12}$$

For the particulate phase:

$$\frac{\partial \rho_P}{\partial t} + \frac{\partial}{\partial x_j}(\rho_P v_{Pj}) = -\frac{\partial}{\partial x_j}\left(\overline{\rho'_P v'_{Pj}}\right) \tag{13}$$

$$\frac{\partial}{\partial t}(\rho_P v_{Pi}) + \frac{\partial}{\partial x_j}(\rho_P v_{Pi} v_{Pj}) = -\epsilon_P \frac{\partial P}{\partial x_i} + \rho_P g_i + \frac{\rho_P}{\tau_{rP}}(v_i - v_{Pi}) - \frac{\partial}{\partial x_j}\left(\rho_P \overline{v'_{Pi} v'_{Pj}} + v_{Pj}\overline{\rho'_P v'_{Pi}} + v_{Pi}\overline{\rho'_P v'_{Pj}}\right) \tag{14}$$

$$\frac{\partial}{\partial t}(\rho_P C_{PP} T_P) + \frac{\partial}{\partial x_j}(\rho_P v_{Pj} C_{PP} T_P) = -n_P Q_P - \frac{\partial}{\partial x_j} \times \left(\rho_P C_{PP}\overline{v'_{Pj} T'_P} + v_{Pj} C_{PP}\overline{\rho'_P T'_P} + C_{PP} T_P \overline{\rho'_P v'_{Pj}}\right). \tag{15}$$

The resulting Reynolds-averaged equations contain new unclosed terms: Reynolds stresses: $-\epsilon_g \rho_g \overline{v'_i v'_j}$, $-\rho_P \overline{v'_{Pj} v'_{Pi}}$; mass flux: $-\epsilon_g \rho_g \overline{v'_j Y'_s}$; enthalpy flux: $-\epsilon_g \rho_g \overline{v'_j T'}$, $-\rho_P \overline{v'_{Pj} T'_P}$; and so on. Expressing them in terms of mean flow quantities using turbulent models can close these terms. It should be noted that all of the variables in Eqs. 9 to 15 and the ones following represent the mean quantities of vectors or scalars in the reactor, omitting the overbars for simplicity.

In the present study, a modified gas–particle two-phase turbulent model $k-\epsilon-k_P$ is employed (Gao, 1997), in which the gas-phase turbulence model $k-\epsilon$ is corrected to embody the influences on the overall turbulent configuration of comparatively high catalyst particle concentration in the FCC riser reactors. To describe the particulate turbulence, the particle turbulent kinetic energy k_P transport equation is used; the equation also reflects its own turbulent characteristics. The second-order turbulence correlation terms in Eqs. 9 to 15 due to the Reynolds averaging process have been modeled using Boussinesq's gradient hypothesis (Chen and Wood, 1985; Adeniji-Fashola and Chen, 1990) and is based on the hypothesis of turbulence isotropy. Some examples of the closure are given as follows:

$$-\epsilon_g \rho_g \overline{v'_i v'_j} = \mu_T\left(\frac{\partial v_i}{\partial x_j} + \frac{\partial v_j}{\partial x_i}\right) + \frac{2}{3}\epsilon_g \rho_g k \delta_{ij} \tag{16}$$

$$-\overline{v'_{Pi} v'_{Pj}} = v_P\left(\frac{\partial v_{Pi}}{\partial x_j} + \frac{\partial v_{Pj}}{\partial x_i}\right) + \frac{2}{3} k_P \delta_{ij} \tag{17}$$

$$-\epsilon_g \rho_g \overline{v'_j T'} = \frac{\mu_T}{\sigma_T}\frac{\partial T}{\partial x_j} \tag{18}$$

$$-\epsilon_g \rho_g \overline{v'_j Y'_s} = \frac{\mu_T}{\sigma_Y}\frac{\partial Y_s}{\partial x_j} \tag{19}$$

$$-\overline{\rho'_P v'_{Pj}} = \frac{v_P}{\sigma_P}\frac{\partial \rho_P}{\partial x_j}, \tag{20}$$

where $k = (1/2)\overline{u'_i u'_i}$ and $k_P = (1/2)\overline{u'_{Pi} u'_{Pi}}$ are the turbulent kinetic energies for gas and particle phases, respectively. The gas-phase turbulent eddy viscosity, μ_T, is calculated based on the velocity scale ($\sqrt{k}$) and the length scale ($\sqrt{k^3}/\epsilon$):

$$\mu_T = C_\mu \rho_g \epsilon_g k^2/\epsilon. \tag{21}$$

The particle-phase turbulent eddy kinematic viscosity, v_P, is calculated as follows (Zhou et al., 1990; Gou, 1995):

$$v_P = C_{\mu P}\sqrt{k_P k^3}/\epsilon \qquad \mu_P = \rho_P v_P, \tag{22}$$

where ϵ is the dissipation rate of k, and C_μ and $C_{\mu P}$ are constants. The transport equations for k, k_P, and ϵ are given by

$$\frac{\partial}{\partial t}(\epsilon_g \rho_g k) + \frac{\partial}{\partial x_j}(\epsilon_g \rho_g v_j k) = \frac{\partial}{\partial x_j}\left(\frac{\mu_e}{\sigma_k}\frac{\partial k}{\partial x_j}\right) + G_k + G_P - \epsilon_g \rho_g \epsilon \tag{23}$$

$$\frac{\partial}{\partial t}(\epsilon_g \rho_g \epsilon) + \frac{\partial}{\partial x_j}(\epsilon_g \rho_g v_j \epsilon) = \frac{\partial}{\partial x_j}\left(\frac{\mu_e}{\sigma_\epsilon}\frac{\partial k}{\partial x_j}\right) + \frac{\epsilon}{k}\left[C_1(G_k + G_P) - C_2 \epsilon_g \rho_g \epsilon\right] \tag{24}$$

$$\frac{\partial}{\partial t}(\rho_P k_P) + \frac{\partial}{\partial x_j}(\rho_P v_{Pj} k_P) = \frac{\partial}{\partial x_j}\left(\frac{\mu_P}{\sigma_P}\frac{\partial k_P}{\partial x_j}\right) + \frac{\partial}{\partial x_j}\left(k_P \frac{v_P}{\sigma_P}\frac{\partial \rho_P}{\partial x_j}\right) + G_{kP} + G_{gP}, \tag{25}$$

where C_1 and C_2 are empirical constants; σ_k, σ_P, and σ_ϵ are Prandtl numbers for turbulent diffusion of k, k_P, and ϵ; and G_k and G_{kP} are generation rates of k and k_P, respectively.

$$G_k = \mu_T\left(\frac{\partial v_i}{\partial x_j} + \frac{\partial v_j}{\partial x_i}\right)\frac{\partial v_i}{\partial x_j} \tag{26}$$

$$G_{kP} = \mu_P\left(\frac{\partial v_{Pi}}{\partial x_j} + \frac{\partial v_{Pj}}{\partial x_i}\right)\frac{\partial v_{Pi}}{\partial x_j}, \tag{27}$$

G_P is a term in the gaseous turbulent kinetic energy k equation, which reflects the influence of the particle phase with a comparatively high concentration on the gas turbulent configuration, and G_{gP} is the one that changes the particulate-phase turbulence pattern, appearing in the particle turbulent kinetic energy transport equation:

$$G_P = \frac{2\rho_P}{\tau_{rP}}\left(C_P^p\sqrt{k k_P} - k\right) + \frac{1}{\tau_{rP}} v_i \frac{v_P}{\sigma_P}\frac{\partial \rho_P}{\partial x_i} \tag{28}$$

$$G_{gP} = \frac{2\rho_P}{\tau_{rP}}\left(C_P^p\sqrt{k k_P} - k_P\right) + \frac{1}{\tau_{rP}}\frac{v_P}{\sigma_P}(v_i - v_{Pi})\frac{\partial \rho_P}{\partial x_i}. \tag{29}$$

A successful simulation predicting the gas–particle turbulent flows in circulating fluidized beds has been carried out that

corrected the high particle concentration by adding G_P and G_{gP} on the basis of the dilute gas–particle two-phase k-ϵ model and the k_P transport equation.

Constitutive equations

The fluid density, ρ_g (in kg/m^3), is related to the temperature and pressure by the ideal gas law. The particle density, $\overline{\rho_P}$, is set at a constant value. The other properties of the gas phase, such as specific heat capacity, viscosity, coefficient of heat conductivity, and diffusion coefficient, vary with the temperature of the gas phase.

For the term expressing interphase momentum transport in Eqs. 2, 6, 10, 14, 28 and 29, the time scale characterizing the particle response, τ_{rP}, can be defined according to Adeniji-Fashola and Chen (1990) as

$$\tau_{rP} = \frac{d_P^2 \bar{\rho}_P}{18\mu} \frac{1}{C_D} \frac{24}{Re_P}. \tag{30}$$

In this expression the drag-force coefficient for an isolated particle, C_{DS}, depends on the particle Reynolds number Re_P ($\epsilon_g \rho_g d_P |\boldsymbol{v} - \boldsymbol{v}_P|/\mu$) as follows

$$C_{DS} = \begin{cases} 0.44 & Re_P > 1{,}000 \\ \dfrac{24}{Re_P}\left(1 + 0.15 Re_P^{0.667}\right) & Re_P \le 1{,}000. \end{cases} \tag{31}$$

This equation was obtained on the basis of the Ergen equation and empirical correlation according to the void fraction of the particle phase. Assuming $C_D = C_{DS} \cdot \epsilon_g^{-2.65}$, and making an adjustment for the effect caused by the presence of the other particles in the fluid, this expression acts as a correction to the usual Stokes' law for the free fall of a single particle (Gidaspow, 1986). Heat transfer between the gas and particulate phases plays an important role in the catalytic cracking of hydrocarbons. The rate of interphase heat transfer appears as an additional source/sink term in the energy differential equation for each phase as $Q_P = \pi d_P Nu_P \lambda (T_P - T)$, where the heat-transfer Nusselt number, Nu_P, is given by Kunii and Levenspiel (1969): $Nu_P = 0.03 Re_P^{1.3}$, $0.1 < Re_P < 100$. Table 1 gives the empirically assigned model constants in the gas–particle turbulent-flow-reaction model.

Catalytic cracking kinetic model

Modeling of the source term, W_s, in Eqs. 3, 4, 11, and 12 requires input from the catalytic cracking kinetic model. Since the catalytic cracking of petroleum gas oil results in a broad spectrum of products ranging from hydrogen and methane to heavy polymeric material adhering to the catalyst surface as coke, a thirteen-lump kinetic model (Sa et al., 1995), proposed for the riser reactors fed with a blend of gas oil and vacuum residua, is incorporated in the present hydrodynamic reaction model. The kinetics model considers the following lumps according to the structure-group compositions of the feed oils:

P_h = paraffinic parts (heavy fractions)
N_h = naphthenic parts (heavy fractions)
Ah = aromatic parts except FAh (heavy fractions)
FA_h = aromatic parts in resin and asphaltene of vacuum residuum (heavy fractions)
P_m = paraffinic parts (mediate fractions)
N_m = naphthenic parts (mediate fractions)
Am = aromatic parts (mediate fractions)
P_l = paraffinic parts (light fractions)
N_l = naphthenic parts (light fractions)
A_l = aromatic parts (light fractions)
GO = gasoline
GS = cracking gas
CK = coke

where, subscript l refers to fractions boiling between 221 and 350°C (light fractions), subscript m refers to fractions boiling between 350 and 500°C (mediate fractions), while subscript h refers to heavy fractions boiling above 500°C (vacuum residua and recycled slurry).

The choice of the 13-lumped kinetics is arbitrary; however, the 13-lump kinetic model offers a few advantages. It considers coke and cracking gas as two separate lumps, which allows the coke and cracking gas yield in the riser reactor to be predicted. Dividing the aromatic parts of the vacuum residua into two parts, one of which is in resin and asphaltene fractions, the other in saturate and aromatic fractions, is also helpful in reflecting the feed characteristics. It should be pointed out that kinetic models of varying complexity could be easily incorporated in the flow-reaction model, which is configured such that a more appropriate kinetic model can be substituted.

The reaction rate of a gaseous lump S can be deduced into the following expression:

$$W_S = A_0 \cdot \frac{1}{1 + K_h C_{Ah}} \Phi(C_c) \cdot \frac{\rho_g \rho_P}{\epsilon_g} k_S Y_S, \tag{32}$$

where A_0 is the correction coefficient of the initial catalyst microactivity (ratio of used catalyst microactivity to that of

Table 1. Constants of the Gas–Solid Two-Phase Flow-Reaction Model

C_1	1.44
C_2	1.92
σ_k	1.0
σ_ϵ	1.3
σ_P	1.0
C_μ	0.09
$C_{\mu P}$	0.0064
C_P^p	0.80

Table 2. Experimental Test Cases Used for Turbulent Model Validation

Case	1	2
Investigator	Bader et al. (1988)	Yang (1991)
Particle diameter (m)	7.6×10^{-5}	5.4×10^{-5}
Material density (kg/m^3)	1,714	1,545
Riser diameter (m)	0.305	0.14
Riser height (m)	11.505	11.0
Inlet gas axial velocity (m/s)	3.78	4.33
Particle mass flux (kg/m^2/s)	98	10
Inlet particle volume fraction	0.25	0.022

the catalyst employed in the kinetic experiments), $\Phi(C_c)$ is the decay function of the catalyst due to coke depositing on the catalyst surface C_c (Ling, 1992): $\Phi(C_c) = (1 + 0.51C_c)^{-2.78}$.

Boundary Conditions

The inlet boundary conditions are completely specified for all dependent variables for both the gas and particulate phases of the prescribed flow and reaction conditions. At the bottom inlet and the feed nozzle inlet of the FCC riser, all variables for the gas and particulate phases are regarded as being uniform, except that the prelifting steam (fluidization medium) at the bottom inlet enters with a nonuniform velocity profile determined by $u_m(r) = 1.2245\bar{u}_g(1 - r/R)^{1/7}$. The temperature of both phases and the gaseous composition are set, while the solids velocity follows from the imposed solids mass flux G_s (in kg/m^2/s). Inlet values of k and ϵ were obtained according to Rizk and Elghobashi (1989): $k_{in} = I^2 u_\infty^2$, $\epsilon_{in} = C_\mu^{3/4} k_{in}^{3/2}/l_m$, where, I = turbulent intensity (typically in the range of 0.01–0.05), l_m = integral turbulence length scale equal to $0.1R$, and u_∞ = stream inlet velocity.

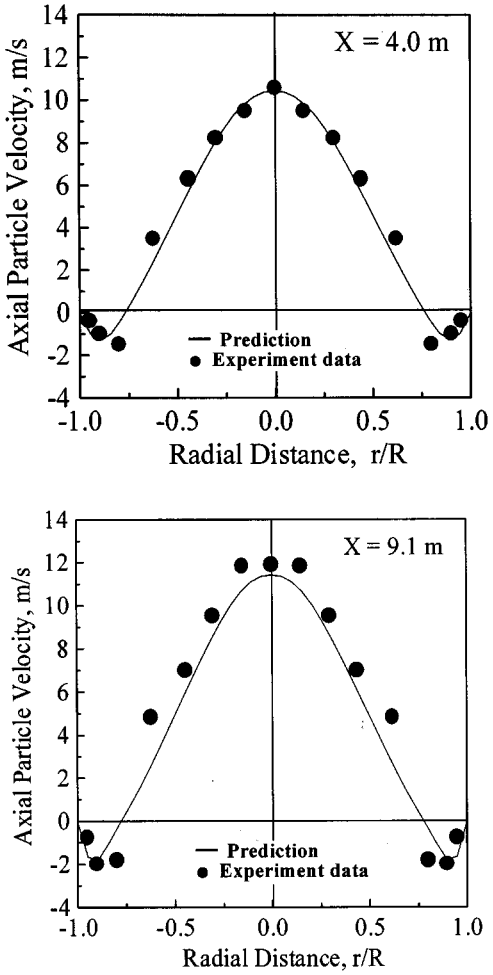

Figure 2. Calculated radial distribution of the axial particle velocity vs. experimental data of Bader et al. (1988).

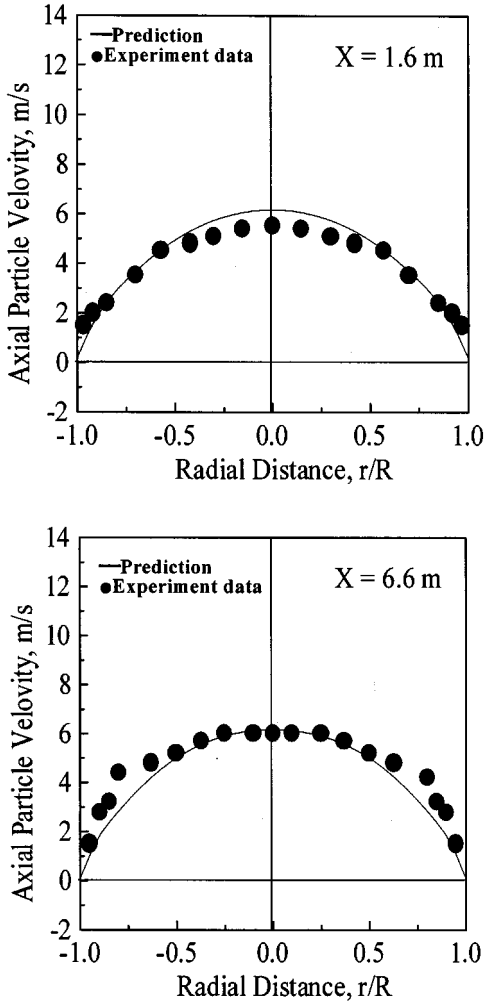

Figure 3. Calculated radial distribution of the axial particle velocity vs. experimental data of Yang (1991).

As the outlet and symmetry plane, the normal gradient of these quantities is set to zero and exit pressure is specified. At the wall surface, the normal gradient of all scalar variables and radial velocities of both phases is also set to zero. For the axial and tangential directions, the gas velocity obeys the "no-slip" boundary condition, and shear stresses are computed from the appropriate "wall function" (Launder and Spalding, 1972), whereas the particulate phase is allowed to slip along the wall. The particle phase velocity gradients at the riser wall have been given by Soo (1967):

$$u_P = L_P(\partial u_P/\partial r)|_{r=R}, \qquad w_P = L_P(\partial w_P/\partial r)|_{r=R},$$

where L_P is the free movement path of particles, defined as $L_P = d_P/\epsilon_P^{1/3}$.

Computational Approach

The set of partial differential equations that express the conservation of momentum, heat, and chemical species at steady state for both phases have been converted to a finite

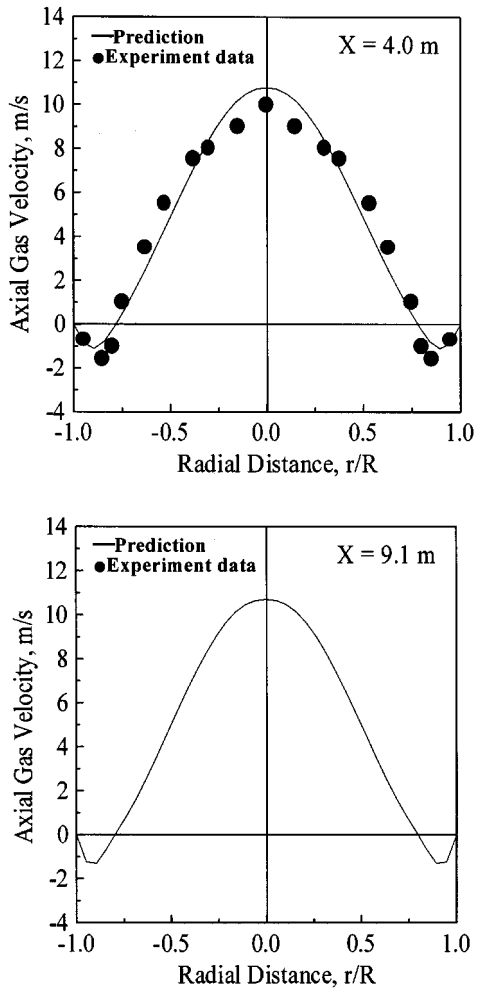

Figure 4. Calculated radial distribution of the axial gas-phase velocity vs. experimental data of Bader et al. (1988).

difference. It can be solved in 3-D cylindrical coordinates over a grid of control volumes that covers the domain of interest, using a finite volume discretization formulation and a staggered grid (Patankar, 1980). The upwind scheme was used to evaluate the convective transport terms. Multiple iterations were made on a two-way coupling (Eulerian gas and Eulerian particle) to achieve the convergence of the two-phase flow. To obtain the convergence, a false-time relaxation technique was used to compute the steady-state flow pattern. A very tight tolerance was used for the continuity equations to assure mass conservation. For a further check on mass conservation, the inflows at the bottom of the riser were compared with the net upflow at various heights along the riser. Convergence accuracy is shown as follows:

(1) Relative total surplus source of the pressure-correction equation was less than ξ_g for the gas phase

$$\frac{\text{Total surplus source of pressure-correction equation}}{\text{Inlet total gas mass flux}} < \xi_g. \quad (33)$$

(2) Relative total surplus source of the continuity equation was less than ξ_P for the particulate phase

$$\frac{\text{Total surplus source of continuity equation}}{\text{Inlet total particle mass flux}} < \xi_P, \quad (34)$$

where ξ_g was $0.001 \sim 0.005$, and ξ_P was $0.005 \sim 0.01$.

Validation of Gas–Particle Turbulent Model

The gas–particle turbulent model was validated by the turbulent two-phase flow experimental data reported by Bader et al. (1988) and Yang (1991). Table 2 lists the experimental conditions for the test cases used in the comparison. In both experiments, a laser-Doppler velocimeter (LDV) was used to measure the velocity of the air and solid particles in the vertical pipes.

Figure 2 shows typical radial distribution of axial particle velocities along the axial positions of 4.0 m and 9.1 m, respec-

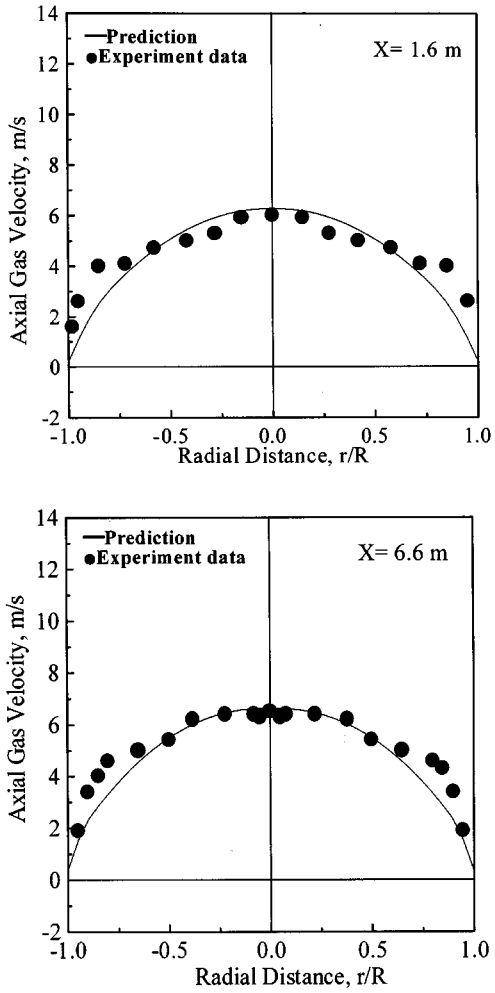

Figure 5. Calculated radial distribution of the axial gas-phase velocity vs. experimental data of Yang (1991).

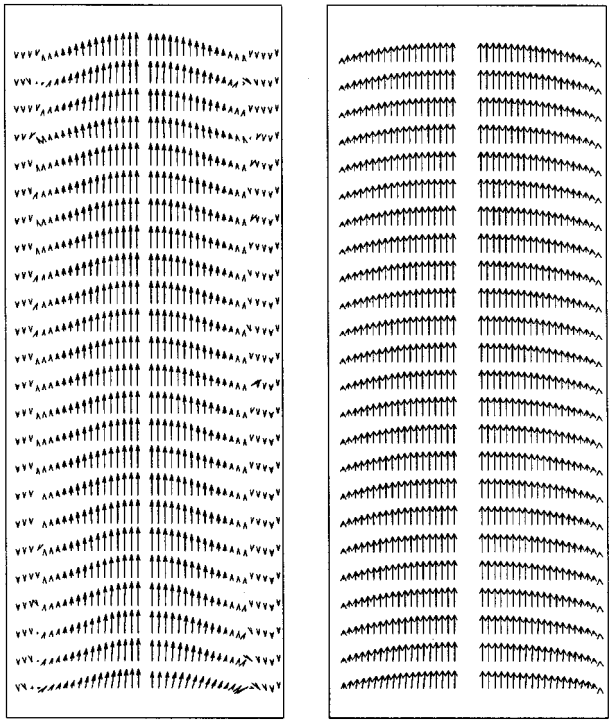

Figure 6. Predicted flow fields of the gas and particle phases in the risers.

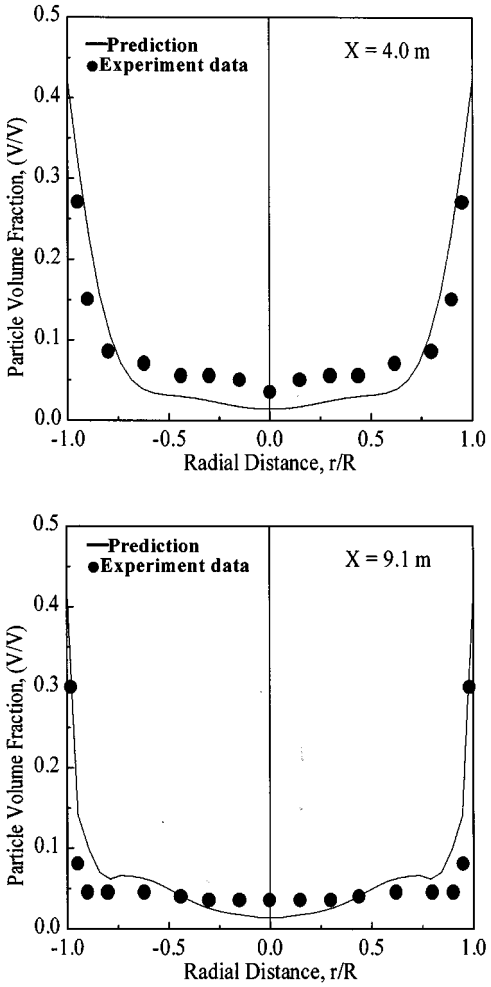

Figure 7. Calculated radial distribution of the particle concentrations vs. experimental data of Bader et al. (1988).

tively, which corresponds to the experimental condition of Bader et al. (1988) at high particulate loading. The particle velocity in the center of the riser was an upward, fast-moving core surrounded by a downward, relatively slow-moving annulus near the wall. The agreement between the predicted and the measured velocities is remarkably good. The particle phase was in an annulus-core type of flow.

Figure 3 is the comparison of the computed radial distribution of the axial particle velocities with experimental results for low particulate loading (Yang, 1991). In this case, the flow pattern for the particles was nearly parabolic due to the low particulate mass flux. Again the agreement between the predicted and the measured velocities is reasonably good, this indicating that the modified two-phase turbulent model developed in the present study is also capable of simulating both the relatively dense and the dilute gas–particle flow in the vertical riser.

Figures 4 and 5 show the comparison of the calculated radial distribution of the axial gas velocity with the experimental data of Bader et al. (1988) and Yang (1991), respectively. Figure 6 shows the prediction of the gas-phase velocity vectors and the particle-phase velocity vectors, which correspond to the experimental conditions of Bader et al. (1988) and Yang (1991). The flow pattern is also a core-annulus type of flow.

Figures 7 and 8 show the radial distribution of particulate concentrations that correspond to the experimental conditions of Bader et al. (1988) and Yang (1991), respectively. In the flow conditions the particle concentrations are all high near the wall of the risers. The comparison between the computed and the actual particle concentration is reasonably good.

In summary, the modified $k-\epsilon-k_P$ two-phase turbulence model developed in this article is capable of simulating the gas–particle flows in FCC risers. The predicted results (such as particulate velocity distribution and particulate concentration distribution) are in good agreement with reported experimental data. The numerical results showed that the flow pattern for both gas phase and particulate phase was a core-annulus type of flow when the particle concentration was high.

Commercial Riser Reactors

Reactor configuration

Figure 9 illustrates the configuration of a FCC riser reactor. In commercial FCC units, regenerated catalyst at a high temperature is lifted into the bottom of the riser reactor by prelifting steam. Feed oil is injected into the riser reactor from feed nozzles uniformly arranged at the side wall with a velocity of about 60 m/s, and the angle between the axis of the riser and the nozzle is typically 30°. Gas and catalyst par-

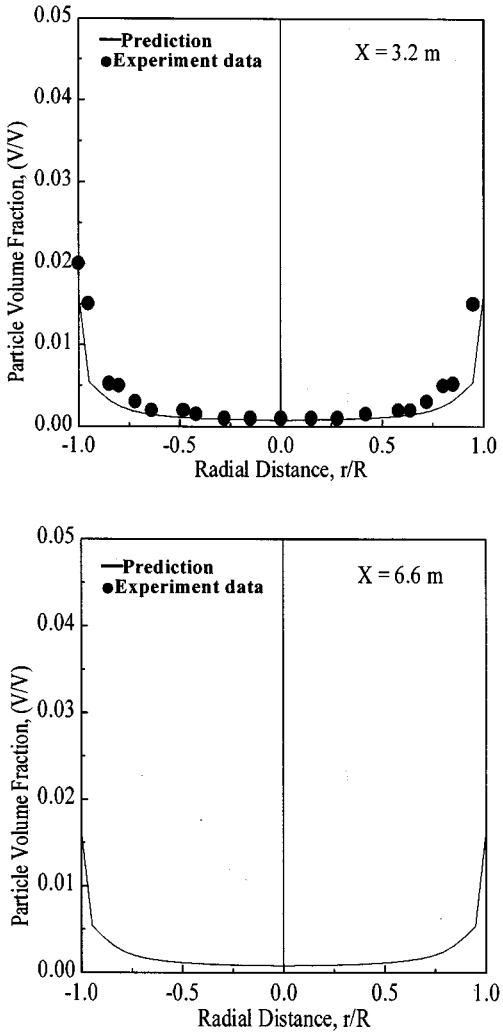

Figure 8. Calculated radial distribution of the particle concentration vs. experimental data of Yang (1991).

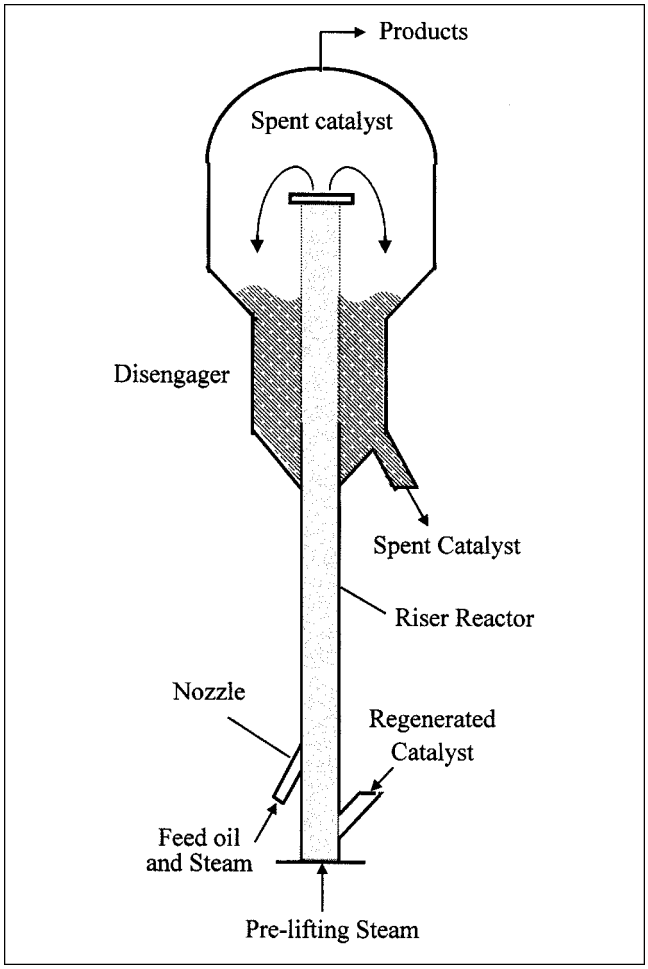

Figure 9. Configuration of an FCC riser reactor.

ticles flow out together at the top of the riser reactor and then separate.

In the present study, a 24×10^4 ton/yr (Unit I) and a 9×10^4 ton/yr (Unit II) vacuum gas oil FCC units were chosen for simulation studies. The dimensions of the commercial riser reactors are listed in Table 3.

Computational scheme

Full 3-D simulation was performed because symmetry is lost as a result of feed injecting mode. Due to the uniform distribution of feed nozzles along the circumference at the feed injecting zone of the reactor, the flow pattern repeated itself in every sector containing one feed nozzle, and the computational integration domain was restricted in the θ-direction to only one sector containing one feed nozzle. For example, only a 90° sector was chosen as the integration domain for Unit I due to four feed nozzles in it. The operating parameters and inlet conditions for the commercial riser reactors are given in Table 4. The computational grid used consists of $75\times10\times15$ mesh cells in the x, r, and θ coordinates (see Figure 10). A total of 11,250 cells were used in the simulation in order to give good resolution to the simulation results. To improve the computational efficiency a coordinate transformation was implemented, generating a fine grid near the inlet zone and a coarse grid in the middle and upper part of the risers.

Results and Discussion

The values of all dependent variables were calculated at the centers of the control volumes all over the riser reactors. Predicted gas–particle turbulent flow and reactions are given in the form of velocity vectors and contours of scalar vari-

Table 3. Dimensions of the Commercial Riser

Size	Unit I	Unit II
L, m	32.8	27.35
H_0, m	15.4	9.9
D, m	0.6	0.4
θ, (°)	30	30
N	4	2

Table 4. Operating Parameters of Commercial Riser Reactors

Items	Unit I	Unit II
Flux of prelift steam (kg/s)	0.034867	0.0464
Inlet temp. of prelift steam (°C)	567.5	602.3
Inlet vel. of prelift steam (m/s)	0.835	1.29
Flux of regen. catalysts (kg/s)	17.361	9.9316
Inlet temp. of regen. catalysts (°C)	567.5	602.3
Material dens. of catalysts (kg/m^3)	1,560	1,500
Inlet vol. fraction of catalysts	0.1885	0.0816
Avg. dia. of catalyst particle (m)	6.6×10^{-5}	6.5×10^{-5}
Inlet vel. of catalysts (m/s)	0.835	0.644
Flux of feed oil (kg/s)	3.6244	2.6833
Inject vel. of gaseous feed oil (m/s)	60.0	60.0
Feed injecting angle (with axis of riser)	30	30
Temp. of the gaseous feed oil (°C)	460	425
Molecular weight of feed oil	420.0	373
Conc. of paraffinic parts of feed oil: CP_m	0.5588	0.6709
Conc. of naphthenic parts of feed oil: CN_m	0.2663	0.0918
Conc. of aromatic parts of feed oil: CA_m	0.1749	0.2373

ables at selected planes of the riser reactors, as shown in Figures 11 to 22.

The results show that the flow in the FCC riser reactors is very complex. Figure 11 presents the flow field of the gas phase at various axial distances of the cross section from the feed inlet plane of Unit II. Figure 12 shows the flow fields of two phases at various vertical planes across the circumferential axis from the feed inlet plane (the axial sections). Figures 11 and 12 show that the feed gas injected into the reactor causes flow inhomogeneities in all directions, especially in the vicinity of the feed nozzles where recycling flows persist. The

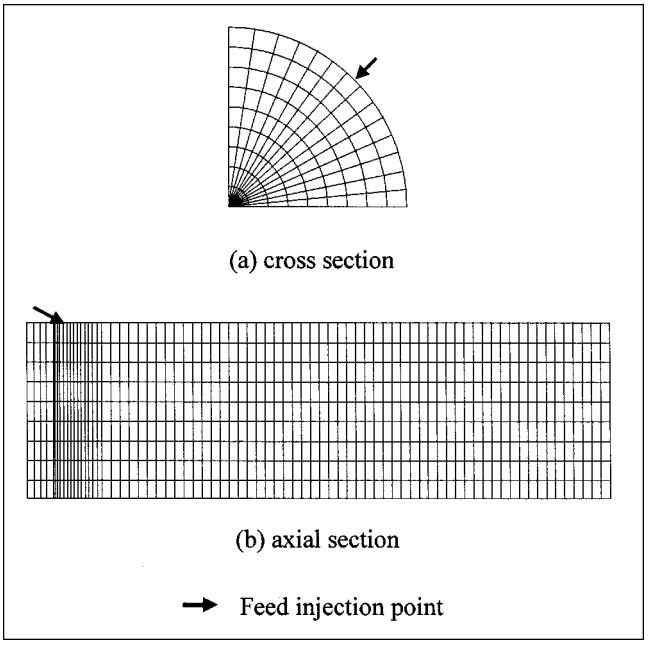

Figure 10. Computational grid for a riser reactor (Unit I).

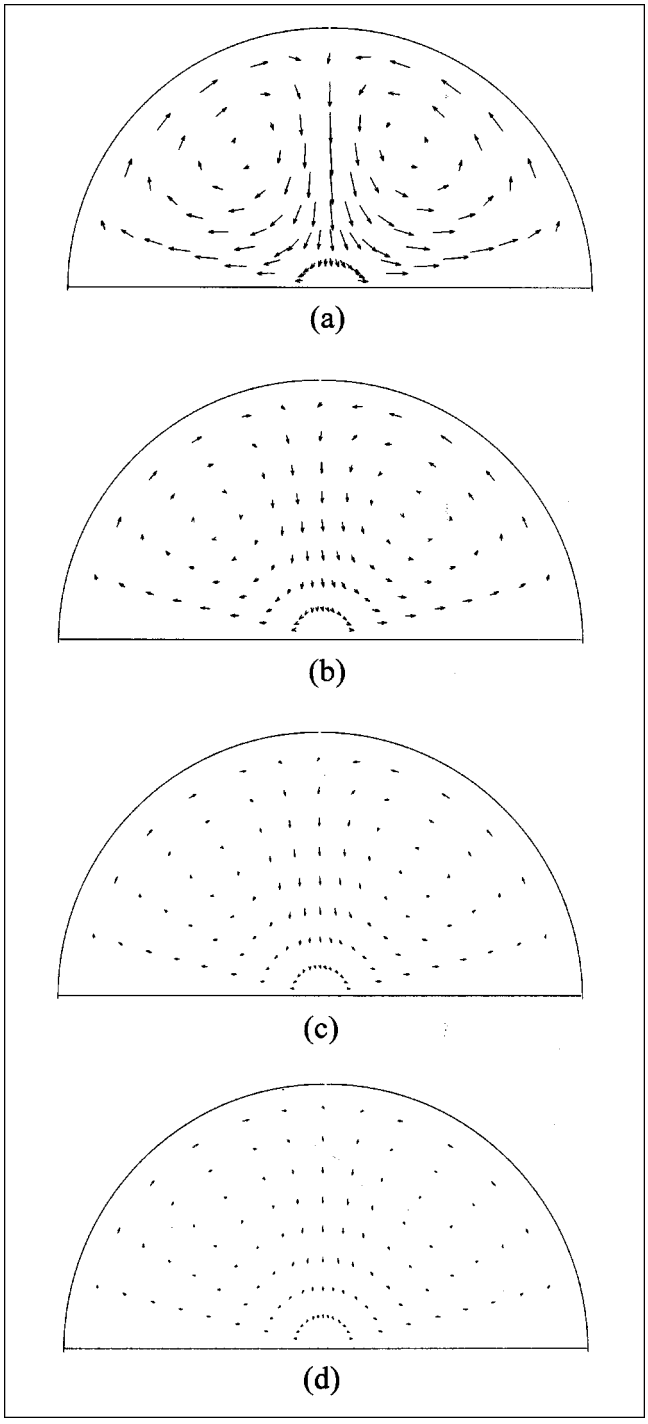

Figure 11. Flow field of the gas phase at various axial distances of the cross-sections from the feed inlet plane of Unit II riser reactor: (a) 1.2 m; (b) 2.4 m; (c) 3.6 m; (d) 4.8 m.

feed injection zone at the riser base is the most complicated part. It is also shown in Figure 12 that the gas phase is directed toward the riser axis from the wall at the axial section across the feed nozzle, nearly parallel with the axis at the vertical plane $\pi/4$ away from the feed inlet plane, and to-

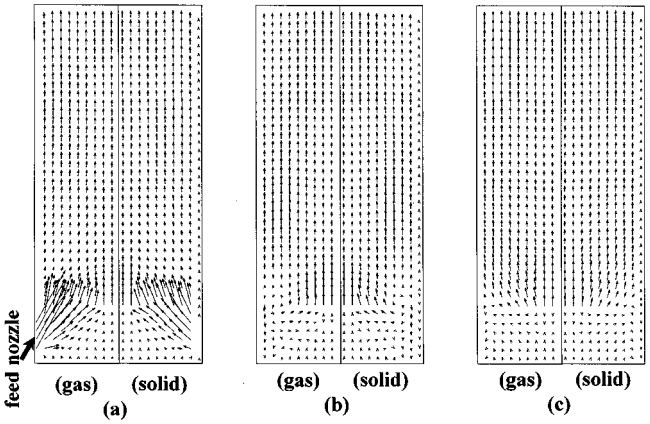

Figure 12. Flow fields of the gas and particle phases at various axial sections of Unit II riser reactor: (a) across feed nozzle; (b) $\pi/4$ from feed nozzle; (c) $\pi/2$ from feed nozzle.

ward the side wall from the axis at the vertical plane $\pi/2$ away from the inlet plane. This corresponds with the recycling flow pattern in Figure 11.

Both phases have almost equal velocities except in the vicinity of the nozzles, where high gas–particle interphase slip is obtained. At the middle of riser reactor, the gas–particle flow becomes more defined along the riser height. The flow recirculation region (eddies at the cross sections) also diminishes. Influences of the feed efflux gradually disappear at this point.

The flow pattern of the catalyst particle is similar to that of the gas phase. However, inhomogeneous distributions of catalyst particulate concentrations are found in all directions. The results given in Figures 13 and 14 show that the particle concentration is less along the axial direction because the

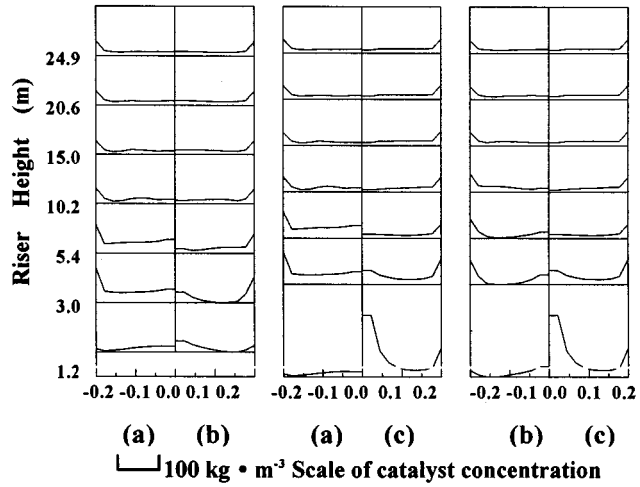

Figure 13. Radial distribution of catalyst concentration at various axial sections of Unit II riser reactor: (a) across feed nozzle; (b) $\pi/4$ from feed nozzle; (c) $\pi/2$ from feed nozzle.

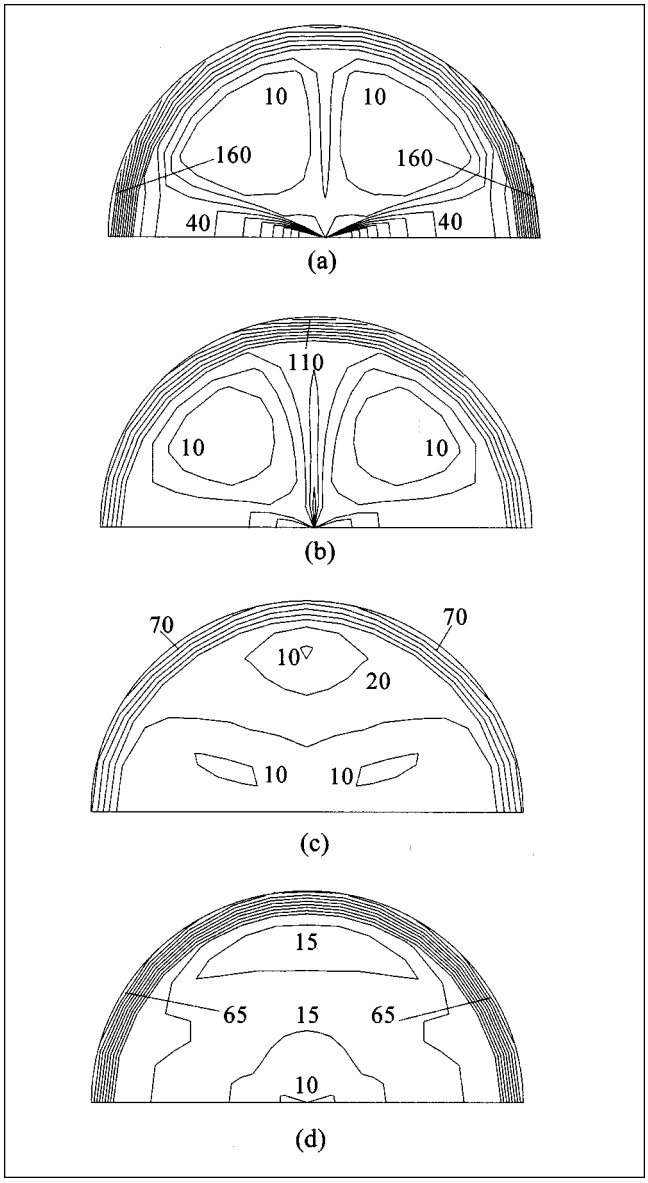

Figure 14. Contour diagram of catalyst concentration (kg/m^3) at various cross sections (Unit II): (a) 1.2 m; (b) 5.4 m; (c) 10.2 m; (d) 15.0 m.

cracking reaction of oil gas resulted in increased gaseous volume. Figures 15 and 16 show contour diagrams of the catalyst particulate concentrations at the cross sections across the feed nozzle. The concentration gradient in the vicinity of the feed nozzle is very high, as expected. In the middle and upper parts of the risers, the distribution of the particle concentration is similar to that in a conventional circulating fluidized-bed riser in the radial direction; there are lower concentrations in the central region and higher near the wall. However, there is a reverse distribution around the axial section of the feed nozzles because of the high-velocity feed efflux. In addition, along the circumference, the gradients of the catalyst particle concentration are high at the bottom of the risers because of the way the feed nozzles are arranged.

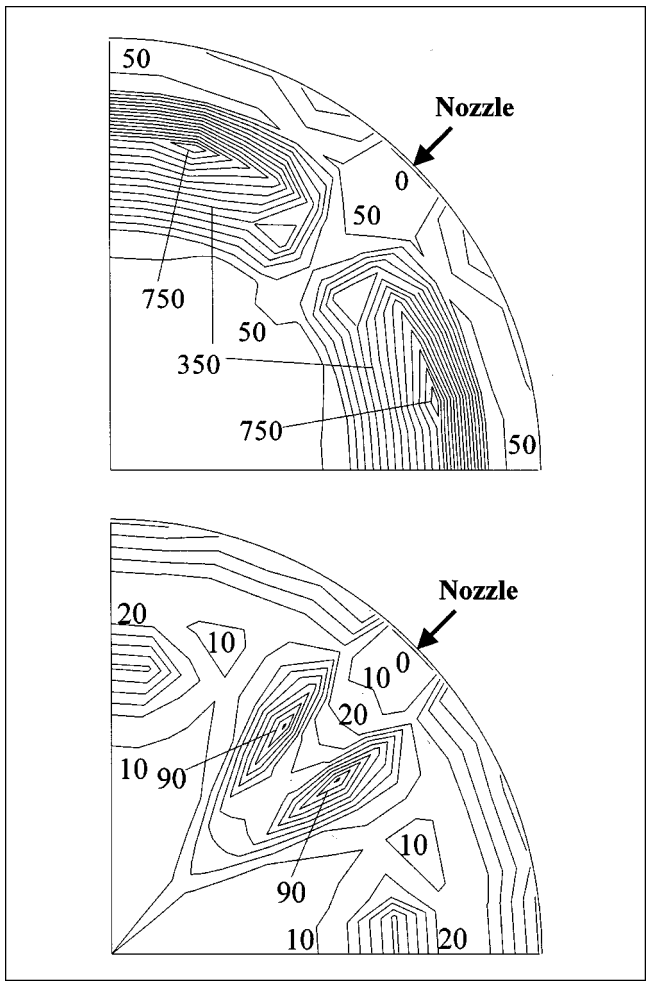

Figure 15. Contour diagram of catalyst concentration (kg/m^3) at various cross sections across feed nozzles of Unit I.

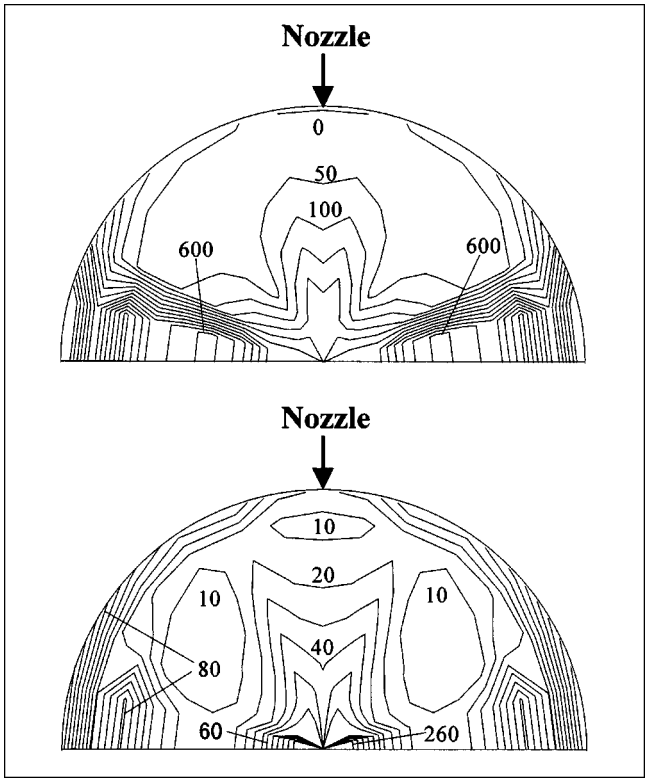

Figure 16. Contour diagram of catalyst concentration (kg/m^3) at various cross sections across feed nozzles of Unit II.

For both phases, nonsmooth distributions of the kinetic energies of the turbulence exist in the three coordinate directions due to the feed gas efflux and the interaction between the gas and particulate phases. Figure 17 shows the radial distribution of the kinetic energies of the turbulence of both phases at various vertical planes across the axis. The kinetic energies of the turbulence of both phases change greatly near the feed nozzle, and a smooth turbulence kinetic energy distribution is obtained along the riser height. Although there are some differences in the kinetic energies of the turbulence between the two phases, their distribution patterns are similar, reflecting a significant interaction between the gas and particulate phases.

The complex flow pattern of the riser reactor has a major impact on temperature distribution. Predicted results show that the two phases have almost the same temperature, and the differences of both phases are less than 1°C, except in the feed inlet area. This agreed with the view of Chen and Cao (1995). Similar temperature distributions of both phases show that the turbulent flow promotes the interphase heat transfer, which is advantageous to catalytic cracking. Large inhomogeneities in temperature distribution are observed in all directions. The area of the feed nozzles is a special area, where a low-temperature region is caused by the endotherm of feed gas temperature rising (see Figure 18).

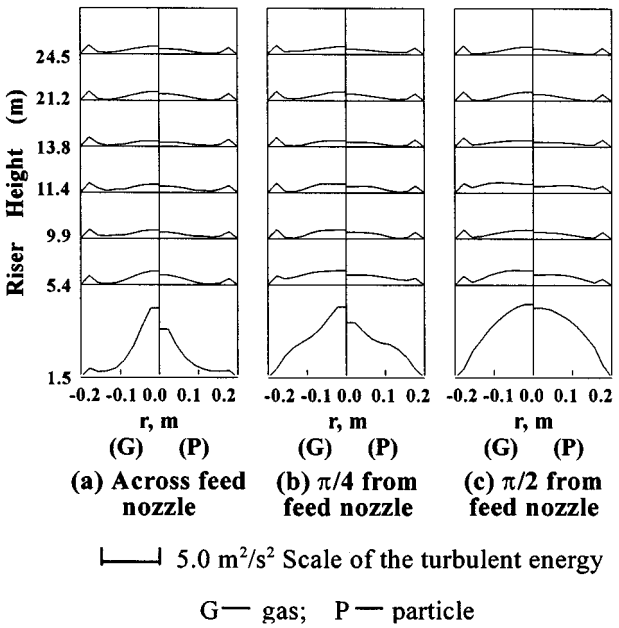

Figure 17. Radial distribution of gas–solid phase turbulent energy at various axial sections of Unit I reactor along the riser height.

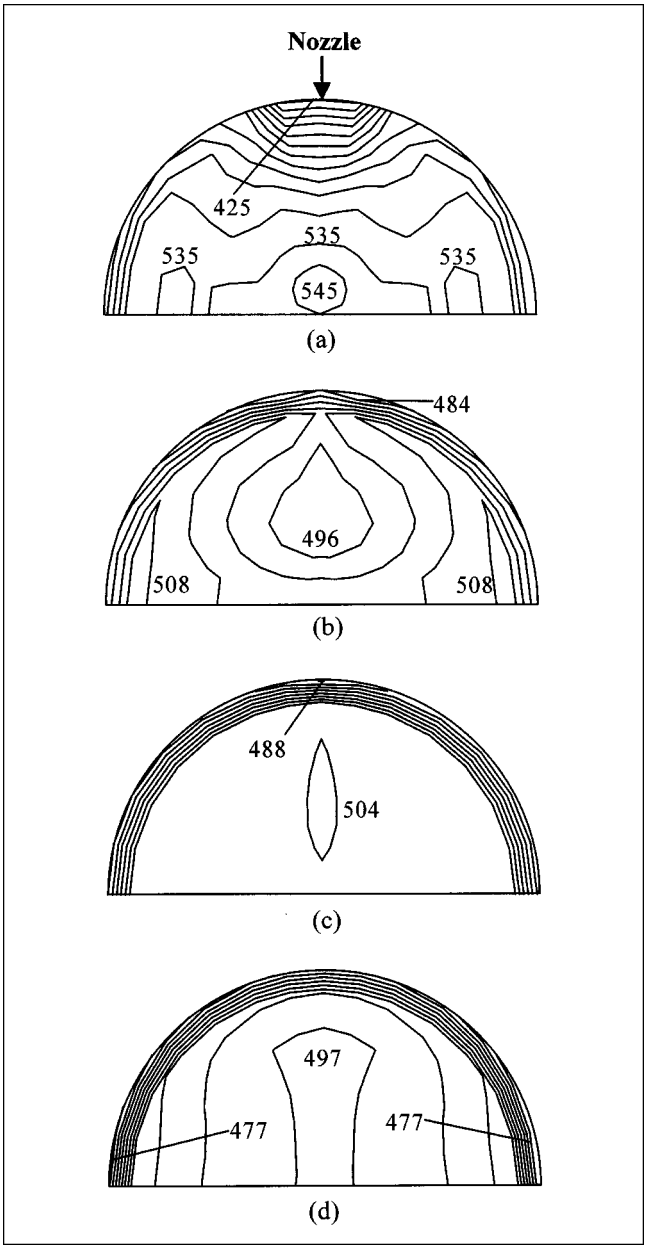

Figure 18. Contour diagram of gas temperature (°C) at various cross sections of the riser reactor (Unit II): (a) 0.0 m; (b) 1.2 m; (c) 3.0 m; (d) 15.0 m.

The temperature distribution away from the feed efflux region and along the riser height becomes more defined. The reason for this pattern of temperature distribution is the two-phase gas–particle flow. Large flow inhomogeneities lead to a high-temperature gradient, while a more uniform flow pattern leads to a more uniform temperature distribution. Figure 19 shows the predicted mean temperatures of both phases along the height of the Unit II riser. A sharp temperature decrease in the feed inlet zone is caused by the necessity of increasing the feed temperature from its boiling point to the two-phase mixture temperature.

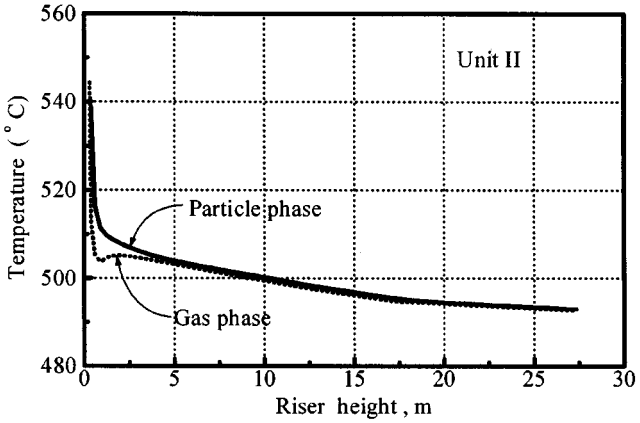

Figure 19. Temperature distribution of gas and solid phases along the riser height (Unit II).

A further gentle decrease in the mixture temperature is caused by the endothermic cracking reaction. The trend of the predicted temperature distribution along the riser reactors is consistent with reported values for commercial riser reactors (Yen et al., 1985).

The 13-lump cracking kinetics was incorporated to determine the progress of the cracking reactions and the distributions of the product yields over the entire riser reactor. The results show that all of the gaseous components have comparatively high concentration gradients in all directions, especially at the riser bottom. As an example, the concentration distributions of gasoline are presented in Figures 20 and 21 (for Unit II). It can be seen that a low gasoline concentration occurs in the vicinity of the feed inlet nozzles. Where the

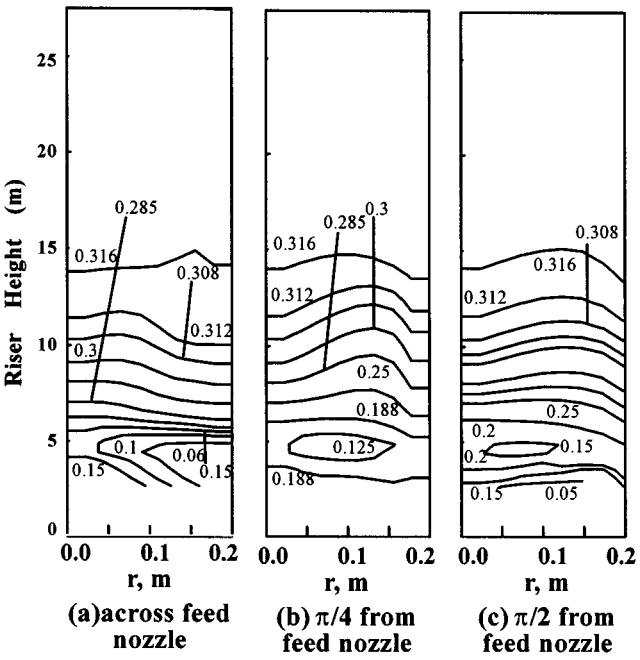

Figure 20. Contour diagram of gasoline concentration at various axial sections (Unit II).

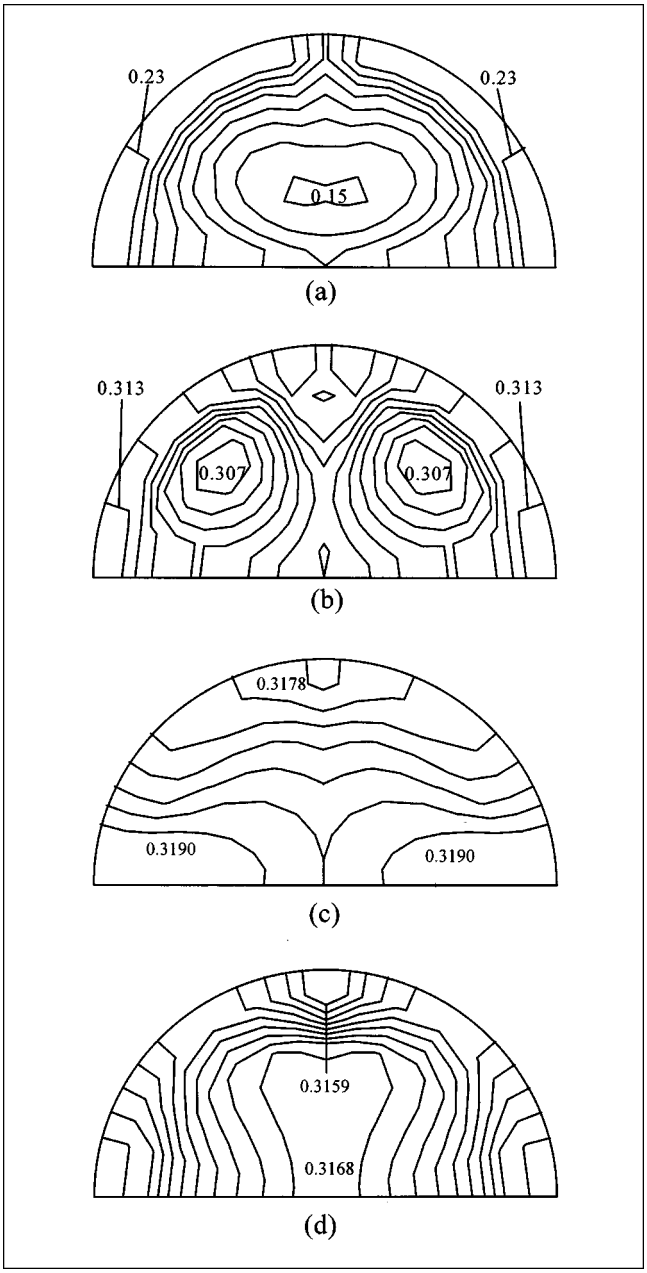

Figure 21. Contour of gasoline concentration at various cross sections of riser reactors (Unit II): (a) 1.2 m; (b) 5.4 m; (c) 15.0 m; (d) 20.6 m.

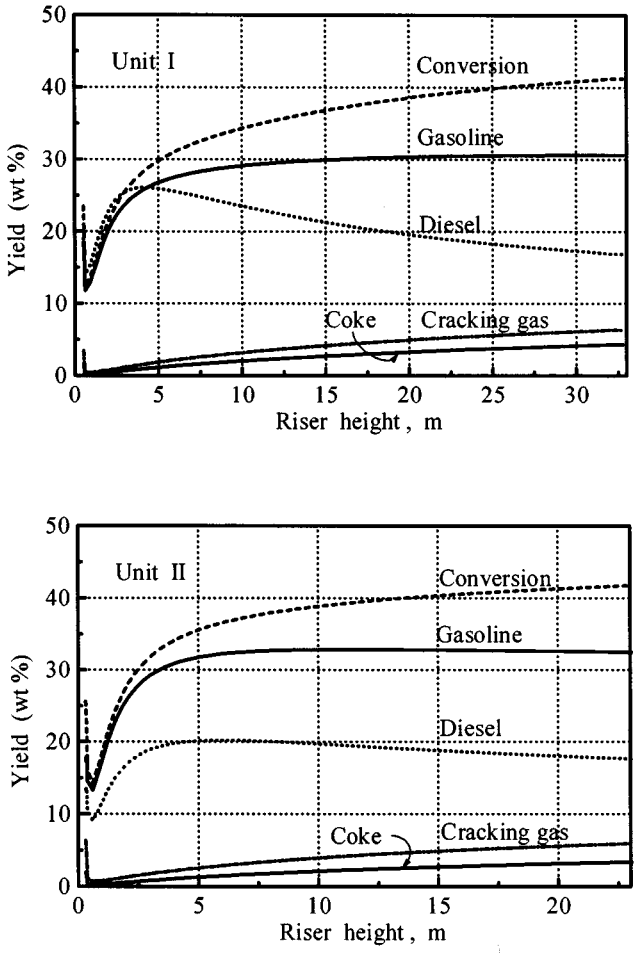

Figure 22. Composition distribution of gas phase along the riser reactor height.

velocity is high, the concentration of the catalyst particle is low, and the mixture temperature is low and is detrimental to cracking reactions. A high gasoline concentration can be found in other regions, which correspond to appropriate cracking reaction conditions, such as high temperature and catalyst concentration.

Figure 22 shows the distribution of the conversion and gaseous component yields averaged over the cross section along the height of the riser for the two reactor units. The catalytic cracking reactions are essentially completed at about one-third of the riser height. After that, the reactions progress gradually (Venuto and Habib, 1978); this behavior is predicted as shown in Figure 22.

In Figure 22 the conversions and yields of the cracking gas and coke for both units increase gradually along the riser height, but the light fuel oil yield reaches a maximum rapidly and begins to decline due to the secondary cracking reaction. Gasoline yield reaches a maximum at about one-third the riser height and remains constant to two-thirds of the riser height, then decreases slightly at the riser exit for Unit II. For Unit I, gasoline yield reaches a maximum at about half the riser height and then remains constant at the riser exit. The gasoline yield distribution of Unit II shows that the gasoline formation rate is higher than its cracking rate in the lower third of the riser height, nearly equal at the middle part, and overcracking to cracking gas and coke in the upper part. The difference in gasoline yield between these two units is mainly ascribed to the feed properties; concentrations of paraffinic and naphthenic components in the feed oil of Unit I are 61.2% and 28.1%, respectively, and for Unit II are 70.2% and 11.2%. The paraffinic component has a higher rate of cracking into gasoline than does the naphthenic component. It also shows that the lumping kinetics for the feed oil used in the turbulent flow-reaction model is adequate, which shows the effect of the feed properties on product yield.

Table 5. Predicted vs. Actual Temperatures and Yields at the Exit of the Riser Reactors

Units	Items	T_{out} (°C)	Heavy Fuel Oil (wt. %)	Light Fuel Oil (wt. %)	Gasoline (wt. %)	Cracking Gas (wt. %)	Coke (wt. %)
Unit I	Predicted	503	41.9	16.9	30.6	6.3	4.3
	Actual	504	42.0	18.5	27.9	7.7	3.9
Unit II	Predicted	493	40.5	17.2	32.3	6.4	3.6
	Actual	496	40.4	18.8	29.7	7.8	3.3

To validate the model, Table 5 compares the predicted temperatures and yields at the riser exit with those of commercial operations. The good agreement of predicted and measured values in Table 5 suggests that the derived model adequately simulates the performance of commercial riser reactors.

Operation Modification Study

As shown in Figure 22, the gasoline yield of Unit II reaches a maximum at about one-third the riser height and remains constant at two-thirds of the riser height, then declines slightly due to overcracking. Figure 23 is a closer view of the gasoline yield distribution along the riser height, in which the gasoline yield reaches a maximum of 32.9 wt. % at the riser height of 11.4 m where the temperature is 498.5°C. At the riser exit, the gasoline yield loses 0.54 wt. %. In order to optimize the desirable FCC products like gasoline, a reaction-terminating technique is considered. A cold liquid medium is injected into the middle or upper part of the riser, where the desired product yield is at its maximum level. The injected liquid is used to reduce the temperature and subsequently to decelerate or stop the overcracking of desirable products to undesirable products like gas or coke.

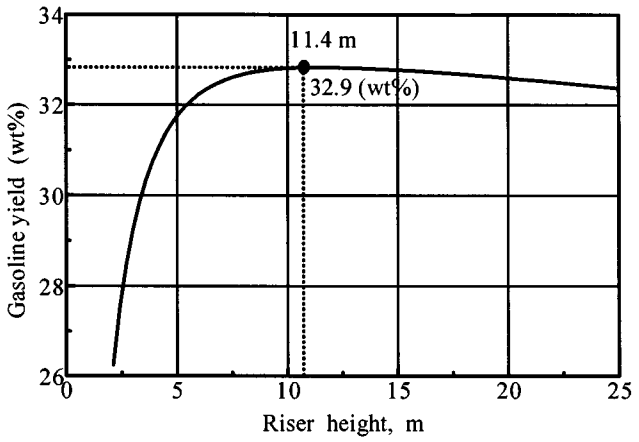

Figure 23. Mean gasoline yield along the riser reactor height: a closer view.

A simulation study on the use of the reaction-terminating technique in commercial riser reactors was carried out for three reaction termination cases using water as the reaction-terminating medium. In Case 1, water is injected at a riser height of 11.4 m, where the maximum gasoline yield of 32.9 wt. % is obtained, by reducing the temperature above the water injecting point. The aim of Case 2 is to increase the regenerated catalyst temperature and raise the temperature under the injecting point, followed by adding water to reduce the temperature above the water injecting point. The aim of Case 3 is to increase the regenerated catalyst flux, thus increasing the catalyst-to-feed-oil ratio, followed by water injection. The computational parameters for the three cases are shown in Table 6 in conjunction with Table 4.

Figures 24 and 25 show the variation in catalyst particle concentrations and gaseous temperatures, respectively, in the injecting region before and after water injection. Significant changes in the gas–particle flow pattern and temperature distribution are observed before and after water injection. The variation in temperature distribution due to the heat requirements raising the temperature and evaporating the water has a significant impact on the catalytic cracking reaction rate and the product yields. Figure 26 shows the mean gaseous temperature distribution along the riser reactor. It can be seen that the temperature distribution can be modified by injecting cold fluid media and/or adding other measurements to achieve a desirable riser-reactor operation. The gaseous temperature profile along the riser height can be divided into two segments by adding a reaction-terminating medium into the riser reactor; this makes it possible to control the bottom mixture and the exit temperature of the riser reactors, respectively, in order to optimize the operation conditions, similar to the mixing temperature control (MTC) technique (Cariou et al., 1989).

Table 6. Computational Parameters

Items	Unit II	Case 1	Case 2	Case 3
Flux (kg/s)	0	0.0882	0.0882	0.0882
Inject velocity (m/s)	0	30.0	30.0	30.0
Temperature (°C)	0	20.0	20.0	20.0
Latent heat for vaporization (J/kg)	0	2,256,300	2,256,300	2,256,300
Evaporation temperature (°C)	0	100.0	100.0	100.0
Specific heat (J/kg/k)	0	4,218.0	4,218.0	4,218.0
Flux of regenerated catalyst (kg/s)	9.9316	9.9316	9.9316	11.91
Inlet temperature of regenerated catalyst (°C)	602.3	602.3	624.7	602.3

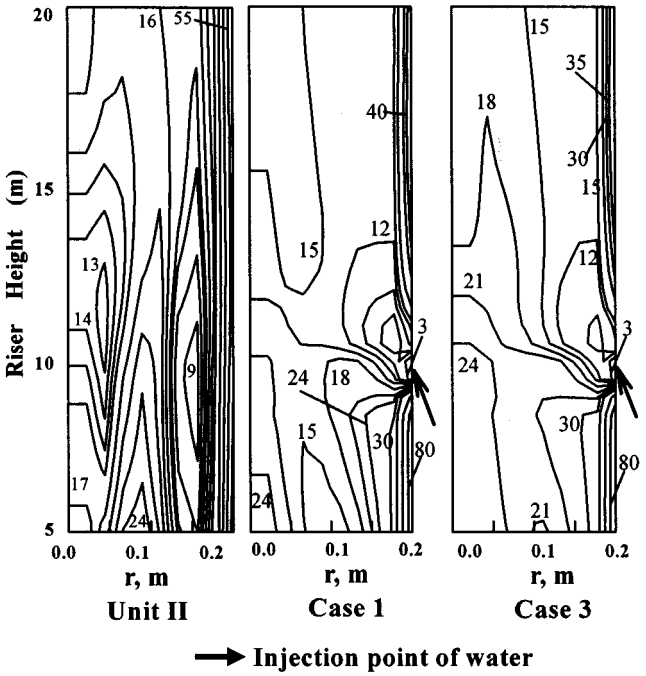

Figure 24. Variation of catalyst concentration (kg/m^3) in the riser before and after injecting water.

The effects of injecting water in various cases on the overall reactor performance are shown in Figure 27. This figure depicts the variation in light fuel oil, gasoline, cracking gas, and coke yields along the riser height, from which distinct changes in all product yields can be seen. These changes resulted from the variation of catalyst concentrations and temperature distribution. The light fuel oil yield increases in all cases. Gasoline yield increases for Case 1, and decreases for Cases 2 and 3. The gas and coke yields are also desirable for Case 1 and undesirable for Cases 2 and 3.

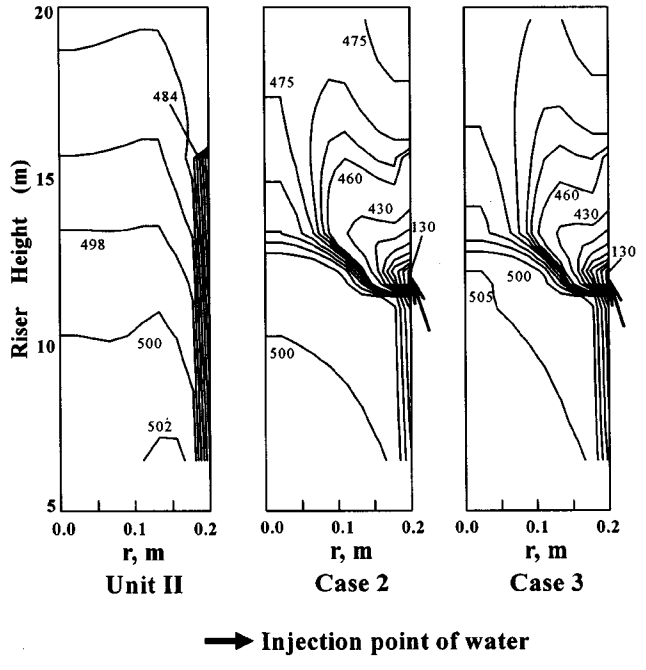

Figure 25. Variation of gaseous temperature (°C) in the riser before and after injecting water.

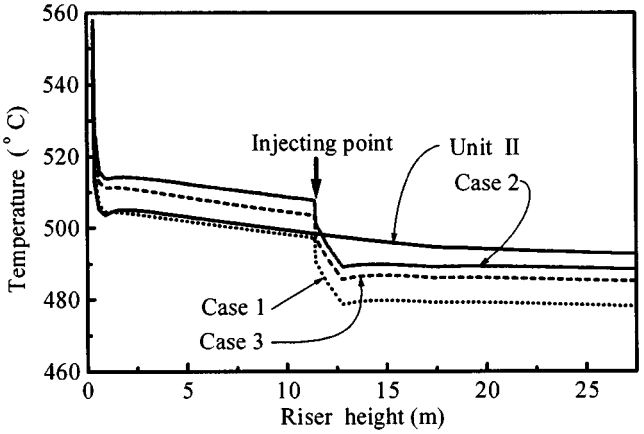

Figure 26. Variation of mean gaseous temperature along the riser reactor height when injecting water.

Table 7 compares the overall yields for various cases with the base-line operation. Case 1 is the best among all cases, with an increment of 0.7 wt. % light fuel oil, 0.6 wt. % gasoline, and a decrement of 0.9 wt. % cracking gas, 0.4 wt. % coke, operating at 13.7°C lower the riser exit temperature. In Case 2, the exit temperature is 4.3°C lower, gas and coke yields decrease 0.2 wt. % and 0.4 wt. %, respectively, the gasoline yield loses 0.6 wt. %, but with a 1.2 wt. % increment of light fuel oil. Case 3 is undesirable because of its 0.6 wt. % decrement of gasoline yield, and 0.4 wt. % and 0.1 wt. % increases of gas and coke yields despite its exit temperature drop of 7.6°C.

To summarize, Case 1 reduces the temperature only above the water injection point. Cases 2 and 3 not only reduce the exit temperature by water injection, but also increase the oil–catalyst mixture temperature at the bottom of the riser reactor by raising the regenerated catalyst temperature or increasing the regenerated catalyst flux. Although the temperature distribution along the riser height is similar between Cases 2 and 3, the results for both cases are very different. In practice, Case 3 increases catalyst flux and raises the oil–catalyst mixture temperature as well as raising the catalyst particle concentration within the riser reactors. Case 2 raises only the oil–catalyst mixture temperature at the bottom of the riser. The impacts of Cases 2 and 3 on the cracking reaction rates can be determined from the following expression (Jacob et al., 1976):

$$r_S = \frac{\Phi(t_C)}{1 + K_h C_{Ah}} \left(\rho_P / \epsilon_g \right) k_S \left(\rho_g \alpha_S \right), \qquad (35)$$

where Case 3 increases (ρ_P/ϵ_g) as well as k_S, but Case 2 varies only k_S. Hence, decreasing only the temperature of the middle or upper parts of the riser can modify the product distributions.

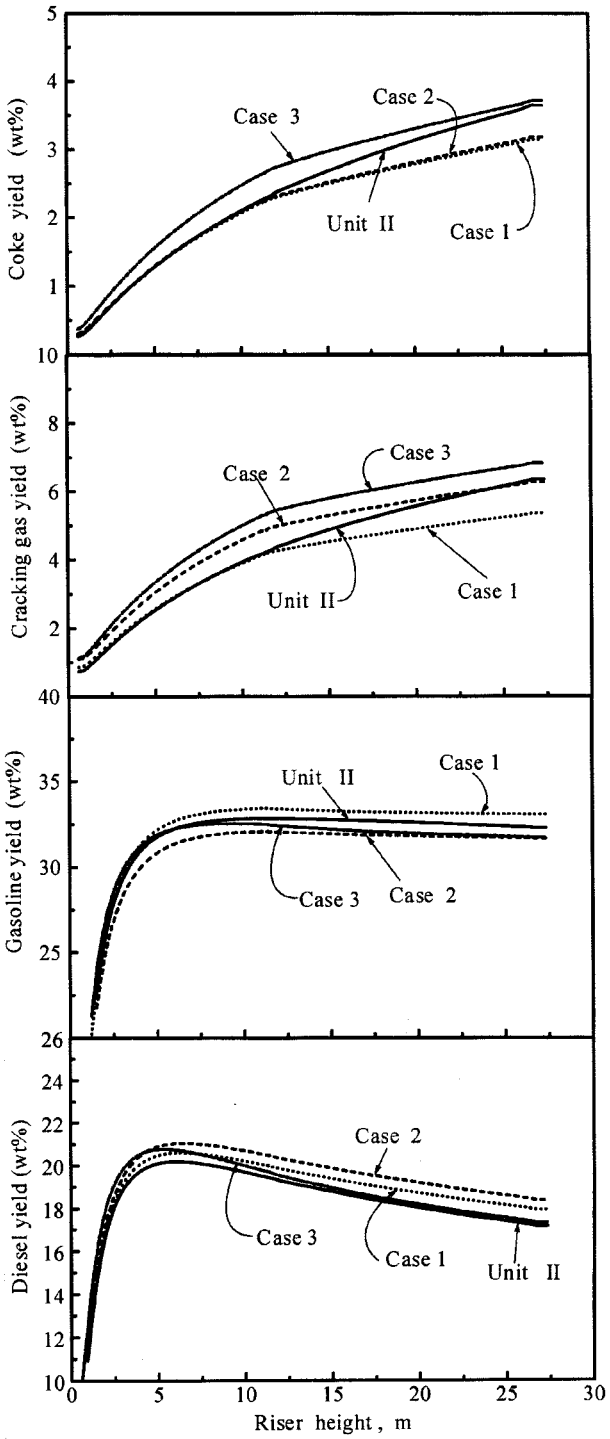

Figure 27. Variation of mean light fuel oil, gasoline, cracking gas, and coke yields along the riser height when injecting water.

Conclusions

A three-dimensional gas–particle turbulent flow-reaction model was developed by incorporating a modified two-phase $k-\epsilon-k_P$ turbulent model and a realistic 13-lump kinetics (Sa et al., 1995). This model can be applied to predict the various key engineering aspects of the two-phase reacting flow in a catalytic riser reactor, including catalyst concentration distribution, the velocity distribution of both phases, interphase slip velocity, the temperature distribution of both phases, and the yield distribution over the entire reactor. The predicted results show that the gas–particulate turbulent reacting flow in the FCC riser reactors is very complicated due to feed efflux. The feed injection zone at the bottom of the riser reactor is the most complex part in respect to the two-phase turbulent flow, heat transfer, and catalytic cracking reactions. The flow fields, particle concentration, temperature distribution, and yield distributions show significant inhomogeneities in the axial, radial, and circumferential directions. Good agreement between the predicted and measured data from the commercial riser reactor indicates that the derived flow-reaction model is an adequate simulation tool for industrial FCC riser reactors.

An operation-modification study for an FCC unit was carried out. It is shown that distribution of the yields is improved by injecting water as the reaction-terminating medium into an appropriate location along the riser reactor, where the yield of desirable products such as light fuel oil or gasoline is maximum. Injection of the terminating medium changes the temperature distribution along the riser and reduces overcracking of desirable intermediate products.

The model derived in this article is based on the assumption that feed gas oil vaporizes instantaneously. Work is currently underway to include evaporation process modeling of feed inside the reactor.

Acknowledgments

The authors gratefully acknowledge the financial support from the China Natural Gas and Petroleum Corporation (CNPC) and the China PetroChemical Corporation (SINOPEC) for this study.

Notation

C_{Ah} = content of aromatic parts in mediate fractions and heavy fractions, wt. %
C_P = specific heat of gas phase, J/kg/K
C_{PP} = specific heat of catalyst particle, J/kg/K
D = diffusion coefficient, m^2/s, diameter of riser reactor, m
d_P = diameter of catalyst particle, m
g_i = gravity component in i coordinate direction, m/s^2
H_0 = length of the disengager, m
k_S = cracking reaction rate constants, m^3/kg catalyst/s
K_h = adsorption coefficient of aromatic parts C_{ah}, 1/(wt. % C_{ah})
L = length of riser reactor, m
n_P = number density of particle phase, $1/m^3$

Table 7. Exit Variables for Water Injection Cases with the Original Prediction

Cases	Heavy Fuel Oil (wt. %)	Light Fuel Oil (wt. %)	Gasoline (wt. %)	Cracking Gas (wt. %)	Coke (wt. %)	Gasoline Selectivity	T_{out} (°C)
Unit II	40.5	17.2	32.3	6.4	3.6	0.764	492.7
Case 1	40.5	17.9	32.9	5.5	3.2	0.791	479.0
Case 2	40.5	18.4	31.7	6.2	3.2	0.771	488.4
Case 3	40.4	17.4	31.7	6.8	3.7	0.751	485.1

N = number of feed nozzles
P = pressure, Pa
Q_P = convection heat transfer flux, J/m^3/s
Q_R = endothermic capacity of the cracking reactions, J/kg
r = radial distance, m
r_S = reaction rate of lump s, mol/m^3/s
R = radius of riser reactor, m
T = temperature, K
t = time, s
t_C = retention time of catalyst, s
$\overline{u_g}$ = superficial velocity of the gas phase, m/s
$v_i v_j$ = velocity components in different coordinates, m/s
X = axial distance of risers, m
$x_i x_j$ = spatial coordinate, m
Y_s = mass fraction of s component
α_s = concentration of lump s, mol/kg
δ_{ij} = unit tensor
ϵ = volume fraction
$\Phi(t_C)$ = decay function of catalyst
λ = coefficient of heat conductivity, W/m/K
μ = kinetic viscosity, kg/m/s
μ_e = effective kinetic viscosity, kg/m/s
θ = angle of the axis and nozzle, deg
σ_T, σ_Y = Prandtl or Schmidt number

Subscripts

g = gas phase
i, j = symbol for spatial coordinates
P = solid phase

Specific symbols

$\overline{}$ = Reynolds time-average value
$'$ = fluctuation value

Literature Cited

Adeniji-Fashola, A., and C. P. Chen, "Modeling of Confined Turbulent Fluid-Particle Flows Using Eulerian and Lagrangian Schemes," *Int. J. Heat Mass Transfer*, **33**, 691 (1990).

Arbel, A., Z. Huang, I. H. Rinard, R. Shinnar, and A. V. Sapre, "Dynamic and Control of Fluidized Catalytic Crackers. 1. Modeling of the Current Generation of FCC's," *Ind. Eng. Chem. Res.*, **34**, 1228 (1995).

Bader, R., J. Findlay, and T. M. Knowlton, "Gas/Solid Flow Patterns in a 30.5-cm Diameter Circulating Fluidized Bed," *Circulating Fluidized Bed Technology*, Vol. II, P. Basu and J. F. Large, eds., Pergamon Press, New York, p. 127 (1988).

Cariou, H., and W. Mauleou, "IFP-TOTAL 'R2R' Technology and Basic Concepts," *Proc. Shanghai Int. Symp. on Technology of Petroleum and Petrochemical Industry*, International Academic Publishers, Shanghai, China, p. 88 (1989).

Chen, C. P., and P. E. Wood, "A Turbulent Closure Model for Dilute Gas-Particle Flows," *Can. J. Chem. Eng.*, **63**, 349 (1985).

Chen, J. W., and H. C. Cao, *Technology and Engineering of Fluidized Catalytic Cracking*, China Petrochemical Press, Beijing, pp. 788 and 864 (1995).

Chen, J. W., "The Development of the Application of Fluidization Technology in China's Petroleum Refining Industry During the Past 20 Years," *Acta Pet. Sin. (Pet. Process. Sect.)*, **1**, 1 (1985).

Chen, L., and H. Weinstein, "Shape and Extent of the Void Formed by a Horizontal Jet in a Fluidized Bed," *AIChE J.*, **39**, 1901 (1993).

Dasgupta, S., R. Jackson, and S. Sundareson, "Turbulent Gas-Particle Flow in Vertical Risers," *AIChE J.*, **40**, 215 (1994).

Gao, J. S., "Numerical Simulation on the Flow, Heat Transfer and Reaction in the Catalytic Cracking Riser Reactors," PhD Diss., Univ. of Petroleum, Beijing, China (1997).

Gates, B. C., J. R. Katzer, and G. C. A. Schuit, *Chemistry of Catalytic Process*, McGraw-Hill, New York (1979).

Gidaspow, D., "Hydrodynamics of Fluidization and Heat Transfer: Supercomputer Modeling," *Appl. Mech. Rev.*, **39**, 1 (1986).

Gidaspow, D., and B. Ettehadieh, "Fluidization in Two-Dimensional Beds with a Jet, Part II, Hydrodynamic Modeling," *Ind. Eng. Chem. Fundamen.*, **22**, 193 (1983).

Guo, Y. C., "A Pure Two-Fluid Model of Reacting Two-Phase Flows and Its Application in Pulverized Coal Combustion," PhD Diss., Tsinghua Univ., Beijing, China (1995).

Hartage, E. U., D. Rensner, and J. Werther, "Solids Concentration and Velocity Pattern in Circulating Fluidized Bed," *Circulating Fluidized Bed Technology*, Vol. II, P. Basu and J. F. Large, eds., Pergamon Press, New York, p. 165 (1988).

Jacob, S. M., B. Gross, S. E. Voitz, and V. W. Weekman, "A Lumping and Reaction Scheme for Catalytic Cracking," *AIChE J.*, **22**, 701 (1976).

Kunii, D., and O. Levenspiel, *Fluidization Engineering*, Wiley, New York, p. 217 (1969).

Launder, B. E., and D. B. Spalding, *Mathematical Models of Turbulence*, Academic Press, London (1972).

Lee, L., Y. Chen, T. Huang, and W. Pan, "Four-Lump Kinetic Model for Fluid Catalytic Cracking Process," *Can. J. Chem. Eng.*, **67**, 615 (1989).

Ling, L., "Influence of Feedstock Composition on the Coke Formation in Residuum Catalytic Cracking," *Proc. Int. Symp. on Heavy Oil and Residue Upgrading and Utilization*, International Academic Publishers, Beijing, China, p. 295 (1992).

Ma, D., and G. Ahmadi, "A Thermodynamical Formulation for Dispersed Multiphase Turbulent Flows," *Int. J. Multiphase Flows*, **16**, 323 (1990).

Mao, X., H. Weng, Z. Zhu, S. Wang, and K. Zhu, "Investigation of the Lumped Kinetic Model for Catalytic Cracking. III. Analyses of Light Fuel Oil Feed and Products and Measurement of Kinetic Constants," *Acta Pet. Sin. (Pet. Process. Sect.)*, **1**, 11 (1985).

Mauleon, J. L., and J. C. Courelle, "FCC Heat Balance Critical for Heavy Fuels," *Oil & Gas J.*, **83**, 64 (1985).

Mcketta, J. J., *Encyclopedia of Chemical Processing and Design, Cracking Catalytic*, Vol. 13, Dekker, New York, p. 1 (1981).

Merry, J. M. D., "Penetration of a Horizontal Gas Jet into Fluidization Bed," *Trans. Inst. Chem. Eng.*, **49**, 189 (1971).

Miller, A., and D. Gidaspow, "Dense, Vertical Gas-Solid Flow in Pipe," *AIChE J.*, **38**, 1801 (1992).

Nieuwland, J. J., M. S. Annaland, J. A. Kuipers, and W. P. M. Swaaij, "Hydrodynamic Modeling of Gas/Particle Flows in Riser Reactors," *AIChE J.*, **42**, 1569 (1996).

Ocone, R., S. Sundareson, and R. Jackson, "Gas-Particle Flow in a Duct of Arbitrary Inclination with Particle-Particle Interactions," *AIChE J.*, **39**, 1261 (1993).

Paraskos, J. A., Y. T. Shan, J. D. McKinney, and N. L. Carr, "A Kinematic Model for Catalytic Cracking in a Transfer Line Reactor," *Ind. Eng. Chem. Process Des. Dev.*, **15**(1), 165 (1976).

Patankar, S. V., *Numerical Heat Transfer and Fluid Flow*, Hemisphere, Washington, DC, p. 146 (1980).

Pita, J. A., and S. Sundareson, "Developing Flow of a Gas-Particle Mixture in a Vertical Riser," *AIChE J.*, **39**, 541 (1993).

Rizk, M. A., and S. E. Elghobashi, "A Two-Equation Turbulence Model for Dispersed Dilute Confined Two-Phase Flows," *Int. J. Multiphase Flow*, **15**, 119 (1989).

Sa, Y., X. Chen, J. Liu, H. Weng, Z. Zhu, and X. Mao, "Investigation of the Lumped Kinetic Model for Catalytic Cracking and the Establishment of the Physical Model," *Acta Pet. Sin. (Pet. Process. Sect.)*, **1**, 3 (1985).

Sa, Y., X. Liang, X. Chen, and J. Liu, "Study on the 13-Lump Kinetic Model for Residual Catalytic Cracking," The Selective Papers in Memorial of 30th Anniversary of the Fluid Catalytic Cracking Process in China, Luoyan Petrochemical Engineering Corporation, Luoyang, China, p. 145 (1995).

Samuelsberg, A., and B. H. Hjertager, "Computational Modeling of Gas/Particle Flow in a Riser," *AIChE J.*, **42**, 1536 (1996).

Saxtoll, A. I., and A. C. Worley, "Modern Catalytic-Cracking Design," *Oil & Gas J.*, **68**, 82 (1970).

Schuurmans, H. J. A., "Measurements in a Commercial Catalytic Cracking Unit," *Ind. Eng. Chem. Process Des. Dev.*, **19**, 267 (1980).

Sinclair, J. L., and R. Jackson, "Gas-Particle Flow in a Vertical Pipe with Particle-Particle Interactions," *AIChE J.*, **35**, 1473 (1989).

Soo, S. L., *Fluid Dynamics of Multiphase System*, Waltham Press (Blaisdell), Boston (1967).

Takatsuka, T., S. Sato, Y. Morimoto, and H. Hashimoto, ''A Reaction Model for Fluidized-Bed Catalytic Cracking of Residual Oil,'' *Int. Chem. Eng.*, **27**, 107 (1987).
Theologos, K. N., and N. C. Markatos, ''Advanced Modeling of Fluid Catalytic Cracking Riser-Type Reactors,'' *AIChE J.*, **39**, 1007 (1993).
Theologos, K. N., I. D. Nikou, A. I. Lygeros, and N. C. Markatos, ''Simulation and Design of Fluid Catalytic Cracking Riser-Type Reactors,'' *AIChE J.*, **43**, 486 (1997).
Venuto, P. B., and E. F. Habib, ''Catalyst-Feedstocks-Engineering Interactions in Fluid Catalytic Cracking,'' *Catal. Rev. Sci. Eng.*, **18**, 1 (1978).
Wang, T., Z. J. Lin, C. M. Zhu, D. C. Liu, and S. C. Saxena, ''Particle Velocity Measurements in a Circulating Fluidized Bed,'' *AIChE J.*, **39**, 1406 (1993).
Weekman, V. W., and D. M. Nace, ''Kinetics of Catalytic Cracking Selectivity in Fixed, Moving and Fluid Bed Reactors,'' *AIChE J.*, **16**, 397 (1970).
Wei, J., and C. D. Prater, *Advances in Catalysis*, Vol. 13, Academic Press, New York, p. 203 (1962).
Wei, J., and C. D. Prater, ''A New Approach to First-Order Chemical Reaction Systems,'' *AIChE J.*, **9**, 77 (1963).
Yang, Y. L., ''Experimental and Theoretical Studies on Hydrodynamics in Cocurrent Upward and Downward Circulating Fluidized Beds,'' PhD Diss., Tsinghua University, Beijing, China (1991).
Yen, L. C., R. E. Wrench, and A. S. Ong, ''Reaction Kinetic Correlation Equation Predicts Fluid Catalytic Cracking Coke Yields,'' *Oil & Gas J.*, **86**, 67 (1988).
Yen, L. C., R. E. Wrench, and C. M. Kuo, ''FCCU Regenerator Temperature Effects Evaluated,'' *Oil & Gas J.*, **83**, 87 (1985).
Zhou, L. X., and X. Q. Huang, ''Prediction of Confined Turbulent Gas-Particle Jet by an Energy Equation Model of Particle Turbulences,'' *Sci. China* (Ser. A), **33**, 428 (1990).
Zhu, K., X. Mao, H. Weng, Z. Zhu, and F. Liu, ''Investigation of the Lumped Kinetic Model for Catalytic Cracking: II. A Prior Simulation for Experimental Planning,'' *Acta Pet. Sin. (Pet. Process. Sect.)*, **1**, 47 (1985).

Manuscript received Oct. 27, 1998, and revision received Mar. 5, 1999.